Modeling of Core Losses in Electrical Machine Laminations Exposed to High Frequency and Non-sinusoidal Flux

Maged Ibrahim

A Thesis

in

The Department

of

Electrical and Computer Engineering

Presented in Partial Fulfillment of the Requirements

for the Degree of Master of Applied Science at

Concordia University

Montréal, Québec, Canada

September 2011

CONCORDIA UNIVERSITY
SCHOOL OF GRADUATE STUDIES

This is to certify that the thesis prepared

By: Maged Ibrahim

Entitled: "Modeling of Core Losses in Electrical Machine Laminations Exposed to High Frequency and Non-sinusoidal Flux"

and submitted in partial fulfillment of the requirements for the degree of

Master of Applied Science

Complies with the regulations of this University and meets the accepted standards with respect to originality and quality.

Signed by the final examining committee:

_____ Chair
Dr. P. Valizadeh

_____ Supervisor
Dr. P. Pillay

_____ Examiner, External to the Program
Dr. M. Packirisamy, MIE

_____ Examiner
Dr. L. A. Lopes

Approved by: _____
Dr. W. E. Lynch, Chair
Department of Electrical and Computer Engineering

_____September 9, 2011_____

_____
Dr. Robin A. L. Drew
Dean, Faculty of Engineering and Computer Science

ABSTRACT

Modeling of Core Losses in Electrical Machine Laminations Exposed to High Frequency and Non-sinusoidal Flux

Maged Ibrahim

Electrical machines account for about 60% of the electricity consumption in industrial countries; hence a huge energy savings could be achieved by even a small increment in the machine efficiency. Improving the designs of electrical machines requires accurate quantification of the machine losses. A significant portion of the losses in electrical machines is caused by the core loss in the magnetic material. The physical mechanism of core losses is still an open problem, and most of the available core loss models are based on limited curve fitting techniques, instead of a physical understanding of magnetic material behaviour.

In this thesis, a new method is proposed to separate the core loss components in laminations exposed to high frequency excitations. Accurate separation of core losses is achieved by calculating the hysteresis energy loss at each frequency, taking into account the flux density distribution. The results highlight that the conventional assumption of constant hysteresis energy loss per cycle is only valid at low frequencies, where skin effect is negligible. In addition to the new separation method, a physics based core loss model is developed to estimate core losses in electrical machine laminations exposed to non-sinusoidal flux. The developed model accounts for the effects of the non-uniform flux density inside the lamination. The model results are verified experimentally by

comparing with the measured core losses in laminations exposed to the flux waveforms in different sections of permanent magnet (PM) and switched reluctance (SR) machines.

ACKNOWLEDGMENTS

The author would like to express his appreciation to his supervisor, Dr. Pragasen Pillay for his invaluable guidance, understanding, and continuous financial support throughout the master's program.

The author would also like to thank all of the other professors and graduate students in the Power Electronics and Energy Research (PEER) group for their consistent support and helpful discussions in the P.D. Ziogas Power Electronics Laboratory.

Lastly, the author would like to express gratitude to his close relatives and friends for their continuous support, and encouragement.

"Special thanks to my parents."

Table of Contents

List of Figures

List of Tables

Chapter 1
Introduction

1.1 The Need for Core Loss Estimation

Electrical machines utilize the majority of the electricity generated in the world. They account for about 45% of the global electricity consumption [1]; hence even a small improvement in machine efficiency can result in significant energy savings. The losses in electrical machines are conventionally divided into five groups: conductor losses, core losses, mechanical losses, and stray losses.

Core losses in electrical machines account for a large portion of the total losses ranging from 15-25% in induction machines operating with sinusoidal supplies [2] and even higher for permanent magnet (PM) machines and switched reluctance (SR) machines. Improving the machine efficiency by design optimization requires accurate quantification of core losses during the machine design stage. The core loss models available in industry require a database of measured core losses in order to achieve accurate core loss quantification. Lamination core loss data are usually provided by steel manufacturers within a limited frequency and flux density ranges. These data are not adequate for the prediction of core losses in high speed electrical machines which require loss information at high frequencies and high flux densities. In addition, the flux waveforms in permanent magnet (PM) and switched reluctance (SR) are naturally non-sinusoidal. This causes an increase in the specific core losses, and makes it difficult to accurately predict the machine losses using the conventional curve fitting models that utilize sinusoidal core loss date.

1.2 Review of Core Loss Models

Core loss modeling has been a subject of interest since the 1800's. Based on an experimental study in 1892, Steinmetz [3] presented his two term formulation for core loss modeling. In his work, the core loss in a magnetic material is considered the addition of hysteresis and eddy current losses. The total core loss is represented by,

$$P = K_h f B^n + K_e f^2 B^2 \tag{1.1}$$

K_h and K_e are the hysteresis and eddy current loss coefficients, which can be extracted from the experimental data, and n is a Steinmetz constant equal to 1.6. This formula is still the most used core loss model in electrical machine design. However, The Steinmetz hysteresis loss flux density exponent n is found to be dependent on the material type, as well as the flux density. The constant hysteresis loss exponent is only applicable for flux densities lower than 1T, which is lower than the flux density level in electrical machines.

The fundamental theory of electromagnetic fields is based on Maxwell's equations,

$$\nabla \times \vec{E} = -\frac{\partial \vec{B}}{\partial t} \tag{1.2}$$

$$\nabla \times \vec{H} = \vec{J} + \varepsilon \frac{\partial \vec{E}}{\partial t} \tag{1.3}$$

$$\vec{J} = \sigma \vec{E} \tag{1.4}$$

$\vec{E}$, $\vec{B}$, $\vec{H}$, and $\vec{J}$ are the electrical field intensity, the magnetic flux density, the magnetic field intensity, and the current density respectively. From the solution Maxwell's equations with an assumption of uniform magnetic field distribution, the eddy current loss coefficient K_e can be expressed as function of the material electrical conductivity σ and

the lamination thickness $2L$ as,

$$K_e = \frac{(2L)^2 \pi^2 \sigma}{6} \tag{1.5}$$

The eddy current loss with the loss coefficient calculated by (1.5) is known as the classical eddy current loss. It has been found that the actual eddy current losses are higher than the calculated classical eddy current losses. The difference is known as the excess losses. The excess losses are traditionally explained by the domain structure and the domain dynamics [3]. Based on the statistical loss theory, Bertotti [4] proposed an additional term to account for the excess losses. Therefore, the Steinmetz core loss formula was modified to,

$$P = K_h f B^n + K_e f^2 B^2 + K_{ex} f^{1.5} B^{1.5} \tag{1.6}$$

where K_{ex} is dependent on the material micro-structure, the conductivity, and the cross sectional area of the lamination. The coefficients of the three-term formulation are generally obtained from the measured core loss data. However, the calculated losses from (1.6) are only accurate within a certain frequency and flux density range. In more recently developed models [5, 6], this range is extended by allowing the coefficients to vary with the frequency and the flux density. However, the determination of these variable coefficients requires additional core loss data at high frequencies and high flux densities.

It has been demonstrated in [7] by means of finite element (FE) simulation that the excess losses are attributed to the non-uniform distribution of the magnetic field inside the lamination resulting from skin effect and the non-linear diffusion of the magnetic flux [8, 9]. Therefore, the total core losses can be represented by the hysteresis and eddy current losses considering the realistic field distribution. The calculation of core losses by FE

simulation is not practical in electrical machine design, which requires fast core loss calculations. An analytical model is reported in [10] to calculate the eddy current loss taking the skin effect into account. However, the loss formula in [10] was found to be only applicable in the low flux density region. Therefore, the formula is not adequate for electrical machine design, as many machines operate in the saturation region.

1.3 Thesis Objective

The objective of this thesis is to achieve a better understanding of the behavior of magnetic materials at high frequency, and to develop a core loss model that that is derived from the physical characteristics of core loss mechanism in magnetic materials, and can quantify the core losses in electrical machine laminations exposed to high frequency and non-sinusoidal flux.

1.4 Thesis Outline

The thesis is divided into five chapters. Chapter two presents a detailed description of the measurement equipment, followed by a comparison of core loss measurements obtained from various standardized test fixtures. Chapter three presents a new method of core loss separation that accounts for the non-uniform magnetic field distribution inside the lamination. The separation method is then employed to investigate the effect of the annealing process on core loss components in laminations exposed to high frequency excitations. In chapter four, an analytical core loss model is developed to predict core losses in electrical machine laminations exposed to non-sinusoidal flux. The model results are then compared to the measured losses in laminations exposed to the flux waveforms in different sections of an inset PM machine, and a 6/4 SR machine. Chapter five concludes the thesis, and proposes future research work.

Chapter 2
Core Loss Measurement

The American Society of Testing and Materials (ASTM) have standardized three test fixtures for core loss measurements: Epstein frame, toroid tester and single sheet tester [11-14]. This chapter compares the measured core losses from the three testers over a wide range of frequencies. Discrepancies in the core loss components (hysteresis and eddy currents), and magnetic permeability measured by the three testers are shown and analyzed.

Core loss measurements are carried out using two test systems; a custom designed commercial system used for sinusoidal core loss measurements, and a test bench developed at Concordia University to carry out core loss measurements in laminations subjected to non-sinusoidal flux.

2.1 Test Fixtures

2.1.1 Epstein Frame

This is the most commonly used test fixture in industry. The Epstein frame is preferred by steel manufacturers because it is easy to assemble, and it has acceptable representation of the magnetic properties of the material. However, the Epstein frame has its own errors. First, the leakage flux around the joints has been found to cause errors [15]. Besides, the assumption of 94cm effective magnetic path length is not an accurate value of the actual flux path length. In order to reduce the effect of anisotropy on core loss measurements, laminations are loaded onto the frame so that longitudinal samples,

cut along the rolling direction, are inserted in opposite limbs, and transverse samples, cut across the rolling direction, are inserted in the other two opposite limbs.

The experimental testing on the commercial system is performed using a 352-turn Epstein frame. The frame is designed to allow core loss measurements for frequencies up to 4 kHz. The experimental testing on the test bench is performed using two Epstein frames; a standard 700-turn Epstein frame for core loss measurements at frequencies lower than 400Hz, and an especially designed 280-turn Epstein frame [18] for higher frequency measurements.

The 700-turn Epstein frame, shown in Fig. 2.1, can be loaded with up to 64 strips. The high number of strips along with the high number of secondary turns induces a secondary voltage with low distortion for core loss measurement at low frequencies and low flux densities as,

$$v_s(t) = -N_s A \frac{dB(t)}{dt} \tag{2.1}$$

where $v_s(t)$ is the instantaneous secondary voltage, N_s is the number of secondary turns, A is the area of the samples, and $B(t)$ is the instantaneous flux density.

It is clear from (2.1) that the 700-turn frame requires high secondary voltage in order to drive the samples to high flux densities at high frequencies. The required induced voltage can be reduced by optimizing the number of turns and the sample's area. Therefore, the 280-turn Epstein frame is used for high frequency testing. The number of turns is reduced to 280 with maximum of one strip per limb, as shown in Fig. 2.2. The frame design allows reaching high flux densities for frequencies up to 6 KHz [19].

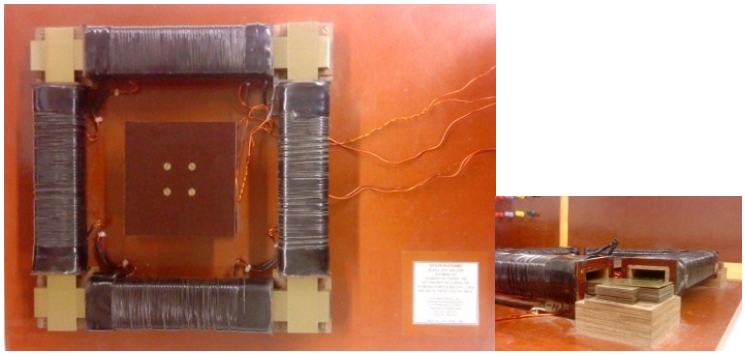

Figure 2.1: 700-turn Epstein frame.

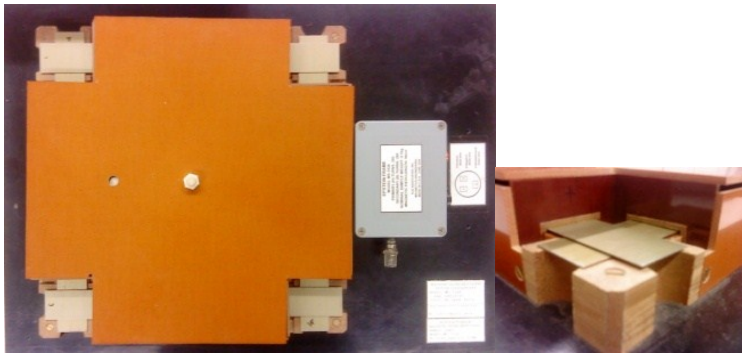

Figure 2.2: 280-turn Epstein frame.

2.1.2 Toroid Tester

The geometry of this tester is similar to the core of radial flux machines, as the flux forms a closed path inside the toroid, thus avoiding the corner effects in the Epstein frame. However, the longer preparation time makes them less desirable.

The design parameters of the toroids are small sample mass and fewer turns to allow high flux densities to be reached at high frequencies, without exceeding the drive capabilities of the measurement equipment. The toroids used for testing with the commercial system have 120 primary turns and 120 secondary turns. The sample width is reduced to 0.415 cm. The design of the toroids aims to keep the primary voltage below the rated voltage of the equipment, while testing at 4 kHz.

2.1.3 Single Sheet Tester

It is the easiest to prepare and setup of the three testers as it only needs one Epstein strip. However, the single sheet tester suffers the same defects of the Epstein frame, as the flux is only measured at the center of strips. The major drawback of this tester is that it is dependent on the results of the Epstein frame and toroid tester for calibration [16].

Experimental testing is performed using a Nickel iron yoke single sheet tester with an effective magnetic path length of 25.4 cm. Measurements performed using the single sheet tester are done separately on one longitudinal sample and one transverse sample, the two test results are then averaged. This method allows good representation of an Epstein frame test.

2.2 Sinusoidal Measurements

The magnetic testing of the samples under sinusoidal excitations is performed using an especially designed commercial Donart test system. The measurements are based on ASTM-A343 [11]. The commercial system, shown in Fig. 2.3, is capable of automatic sinusoidal core loss measurements using the Epstein frame, toroid tester, and the single sheet tester. It is fully customized for high frequency testing with increased drive capabilities of 120V/15A, and enhanced measurement capabilities, as it includes sample temperature monitoring used for testing above 1 kHz. The Epstein frame test has a test frequency range of 20 Hz – 4 kHz. Core loss measurements in this range allow the gathering of core loss data that are not generally provided by steel manufacturers.

Due to the non-linearity of the magnetic materials, when the primary winding of the test fixture is excited with sinusoidal waveforms, the flux density, and therefore the

induced secondary voltage tends to be distorted, especially near saturation. This distortion affects the accuracy of core loss determination, as the peak flux density is used as the reference magnetic quantity. The commercial system uses feedback control to ensure that the secondary voltage remains sinusoidal during saturation. Feedback control is used for testing at frequencies lower than 400Hz. Before each test, the samples are demagnetized by increasing the excitation current slowly until saturation is reached then decreasing it until the sample is free from residual flux.

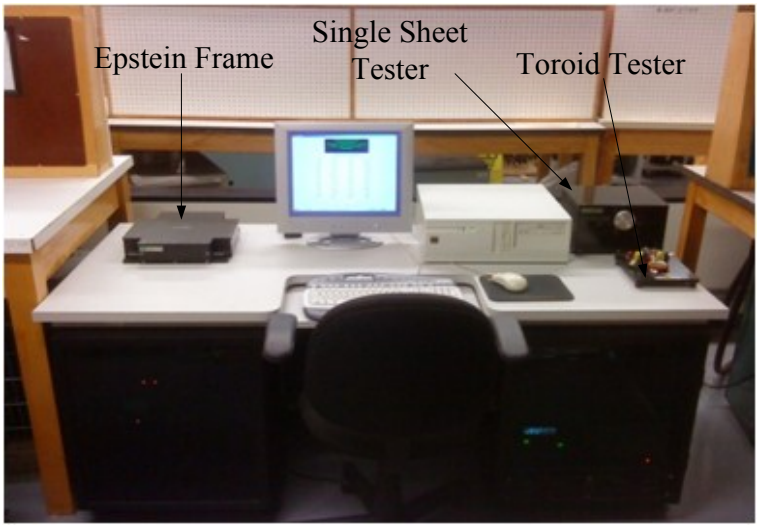

Figure 2.3: Donart test system

2.3 Non-sinusoidal Measurements

This section presents the test bench developed at Concordia University to perform core loss measurements in electrical machine laminations exposed to non-sinusoidal flux. The flux waveforms in electrical machines are obtained by FE simulation. These waveforms are then generated in the laminations, and the specific core losses are measured.

2.3.1 The Need for Non-sinusoidal Core Loss Measurements

The flux waveforms inside many machines, such as PM and SR machines are non-sinusoidal. The estimation of core losses in these machines is a highly non-linear problem, since many factors have to be considered, such as the distribution of magnetic field inside the lamination, minor hysteresis loops, and the flux DC component. Therefore, the sinusoidal core loss data is not sufficient to validate the core loss models used in the design of PM and SR machines. The estimation of core losses is usually done in the post processing stage of the finite element analysis. The core losses at each element is calculated using the established localized flux density waveforms, then the total core loss is calculated by summing the calculated core losses in all the mesh elements. The calculated total core losses can be verified experimentally by comparing to the measured machine core losses. However, this requires building and testing the machine in order to obtain the actual machine core losses, which is impractical during the machine design stage. Also this method does not achieve accurate verification of the core loss models, as the flux density waveforms differ in each part of the machine, and therefore the measured core losses represent the average losses in the machine core.

2.3.2 Test Bench Description

The test bench, shown in Fig. 2.4, uses the Epstein frame to carry out core loss measurements in laminations exposed to non-sinusoidal flux. The system schematic diagram is shown in Fig. 2.5. It uses Matlab Simulink to generate the excitation waveform, and a DSPACE board (DS1103) is used for real time simulation. The excitation signal is sent through a DAC to a high bandwidth amplifier, which excites the Epstein frame primary winding. The core losses are measured using a power meter. A

current probe and a voltage probe are used to measure the excitation current and the induced secondary voltage, respectively. The peak flux density B_p is used as the reference magnetic quantity in the non-sinusoidal core loss measurements [17]. B_p at a certain frequency f can be obtained from the average rectified secondary voltage V_{ave} using [17],

$$B_p = \frac{V_{ave}}{4fN_sA} \tag{2.2}$$

This expression is only valid when there are no minor loops in the main hysteresis loop. Since the minor loops can be produced by the distorted flux waveforms in electrical machines, the instantaneous flux density is calculated from the induced secondary voltage, and the peak flux density is obtained and considered the reference magnetic quantity.

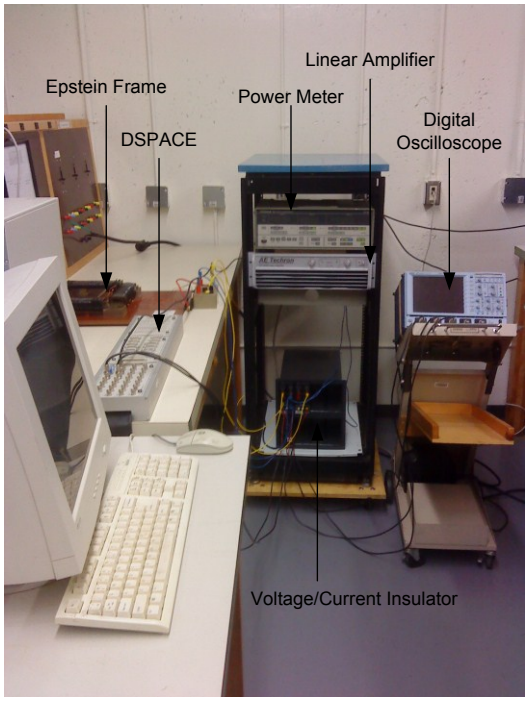

Figure 2.4: Concordia test bench

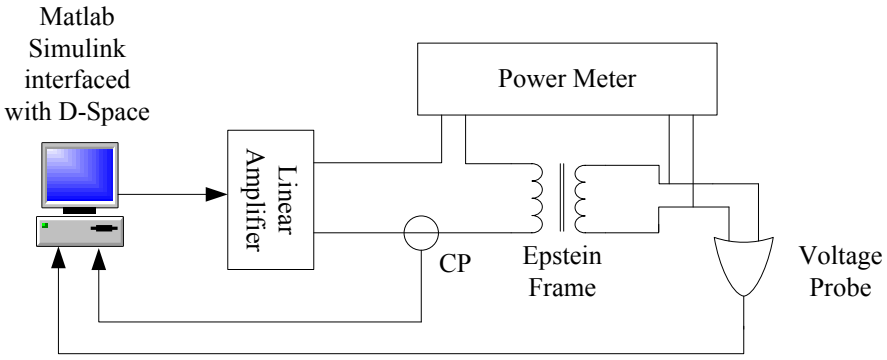

Figure 2.5: Schematic diagram of the test bench.

The test bench is calibrated by comparing sinusoidal core loss measurements with the results obtained from the commercial system using the 352-turn Epstein frame. Core loss measurements for frequencies up to 400Hz are performed using the 700-turn frame, while higher frequency measurements are performed using the 280-turn frame. The results in Fig. 2.6 show good correlation between core loss data obtained from the two systems, with the 280-turn frame achieving higher flux densities at high frequencies.

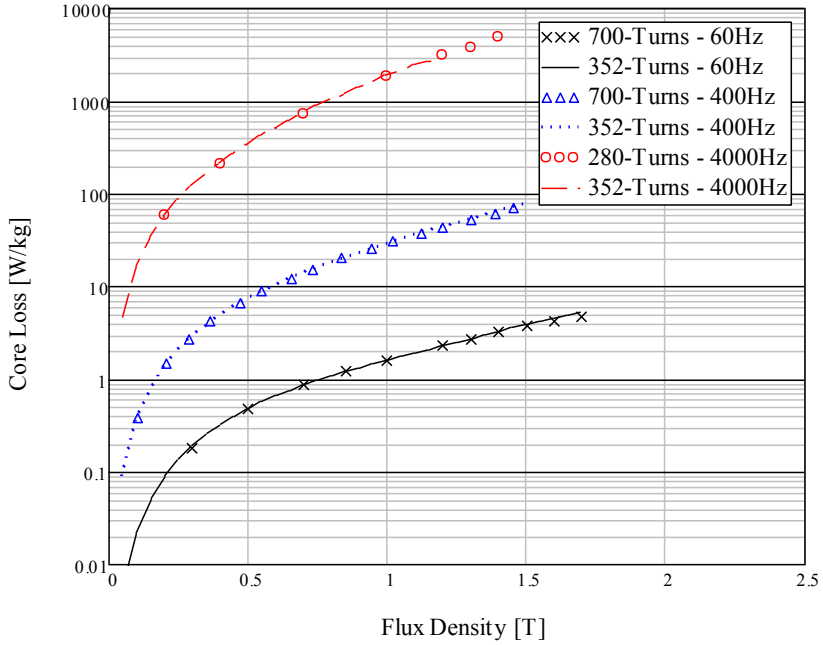

Figure 2.6: Test bench calibration.

2.4 Comparison of Toroid Tester and Epstein Frame Results

Comparative measurements are performed using steel from the same roll arranged into Epstein samples and toroid cores. Core loss components (hysteresis and eddy current) are separated by extrapolating the measured core loss per cycle vs. frequency curves at different flux densities to zero frequency. The hysteresis energy loss per cycle is assumed equal to the power loss at zero frequency. The total hysteresis loss at any frequency is obtained by simply multiplying the extrapolated hysteresis energy loss per cycle by the operating frequency.

From the core loss results, shown in Fig. 2.7, it can be seen that higher losses are measured by the toroid tester for all the testing frequencies from 60Hz to 4 kHz. The higher losses measured by the toroid tester at 60Hz are mainly attributed to the significant increase in the hysteresis loss component in the toroid core, as shown in Fig. 2.8. The increase in the toroid core hysteresis losses has great impact on the measured total losses at low frequencies, where the hysteresis loss is the dominant loss component, as can be seen from the distribution of core loss components, displayed in Fig. 2.9. These higher hysteresis losses are caused by the magnetic damage produced by shearing stress. This has a greater impact on the toroid sample, because it has a lower sample area than the Epstein sample. This magnetic damage can also be observed in the measured magnetic permeability, shown in Fig. 2.10, where it can be clearly seen that the toroid samples have reduced magnetic permeability compared to the Epstein samples. Much of this magnetic damage can be recovered by applying stress relief annealing after cutting the samples [20]. This emphasizes the importance of annealing on the final product for improved

machine efficiency especially for small motors. However, the increased cost makes this prohibitive for low cost commodity products.

From Fig. 2.9 at high frequencies, it can be seen that the hysteresis losses form a smaller portion of the total core losses, but still the measured core losses with the toroid tester are higher than the Epstein frame losses. These higher losses are mainly caused by the higher eddy current loss component in the toroid cores, as shown in Fig. 2.11. The higher eddy currents can be created by the cutting stress which increases the eddy currents in the toroid cores where short circuit paths are introduced on the edges of the laminations. In addition, the reduced magnetic permeability in the toroid samples has a direct impact on the eddy current losses, as the resistance of the eddy current path depends on the effective area of magnetic field. The magnetic field distribution inside the lamination is affected by the magnetic permeability.

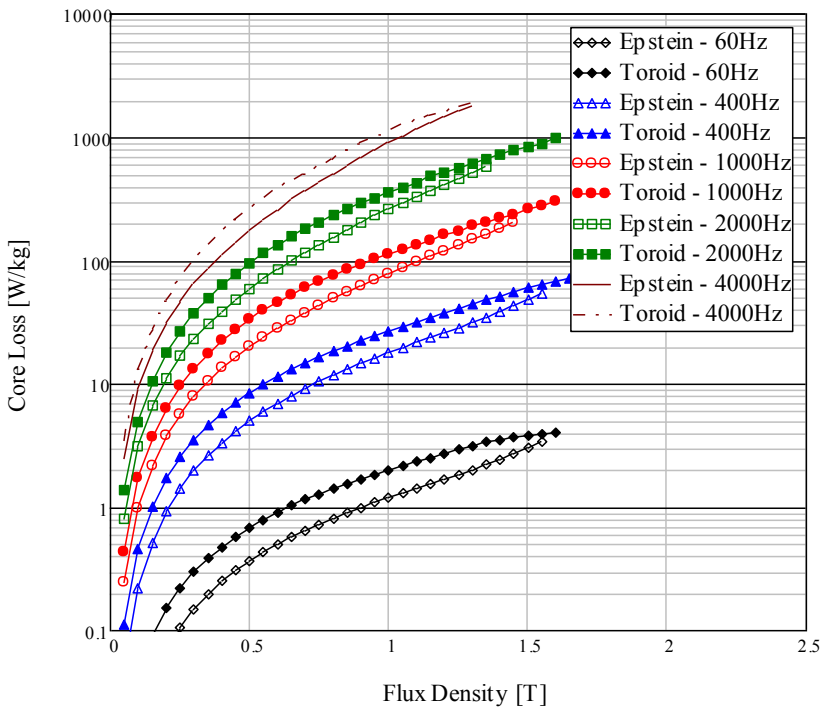

Figure 2.7: Comparison of the core loss measured by the Epstein frame and toroid tester for M19G29.

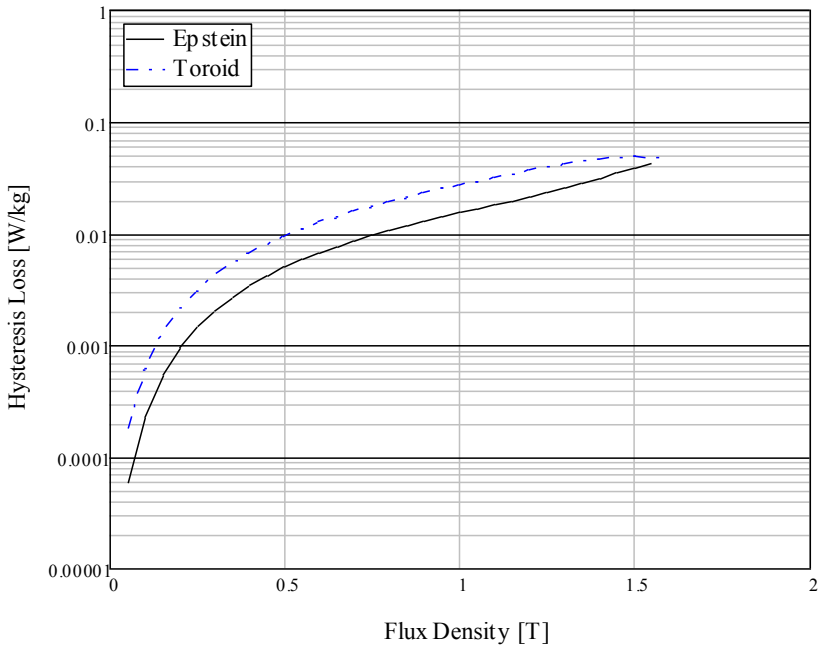

Figure 2.8: Hysteresis energy loss per cycle.

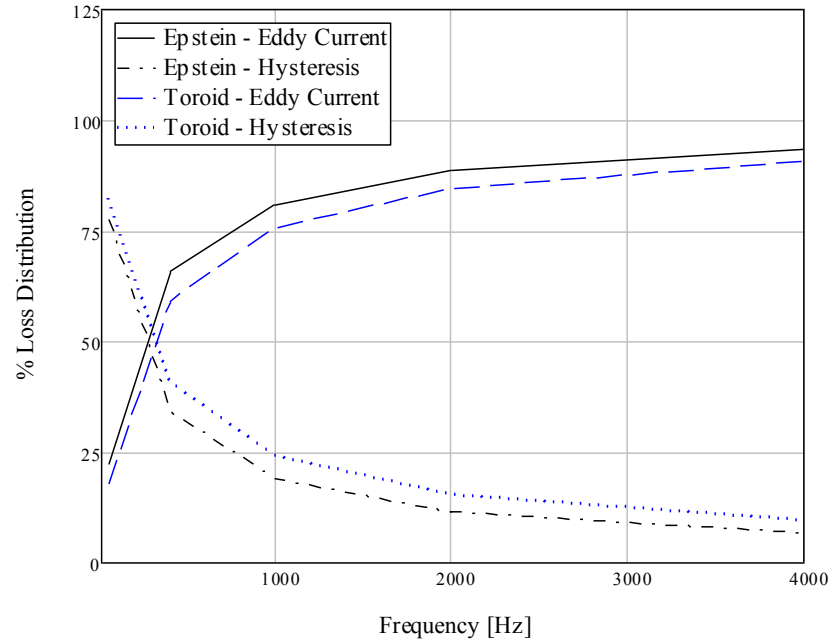

Figure 2.9: Distribution of core loss components at 1T.

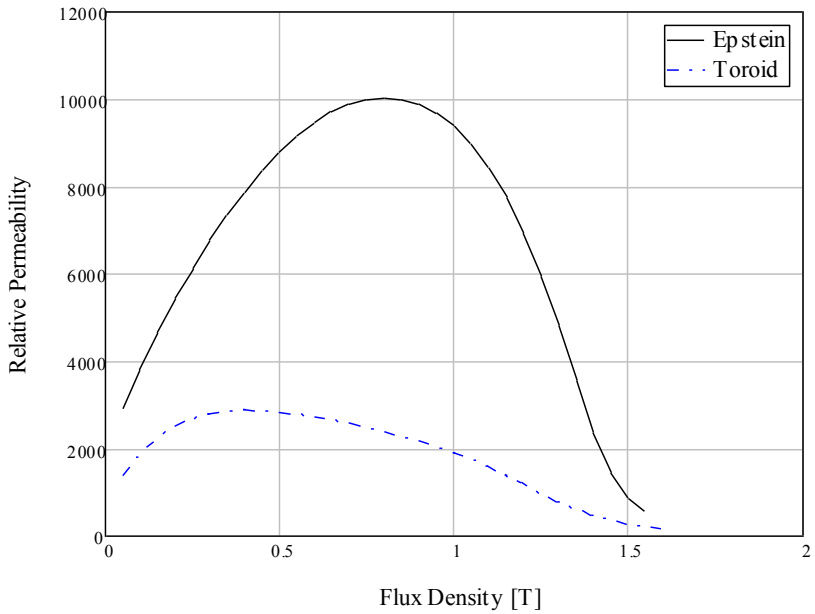

Figure 2.10: Comparison of the magnetic permeability measured by the Epstein frame and toroid tester for M19G29.

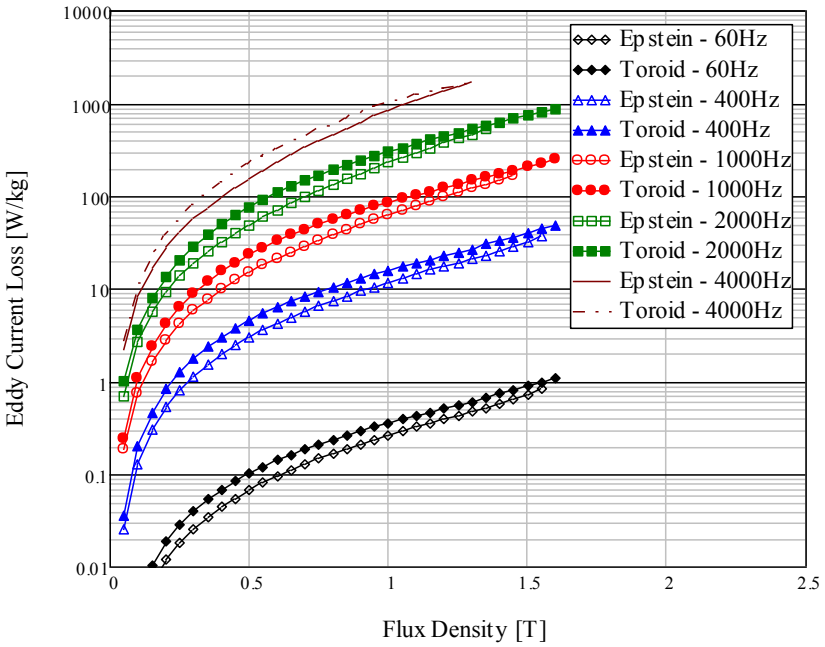

Figure 2.11: Eddy current loss.

2.5 Comparison of Single Sheet Tester and Epstein Frame Results

Comparative measurements are performed using the Epstein frame and the single sheet tester for frequencies from 60Hz to 400Hz. Measurements conducted using the single sheet tester are done on one longitudinal sample and one transverse sample. The results show that the measured core losses are higher in the transverse samples. It can be seen from the separated core loss components in Fig. 2.12 that the increase in the core losses is caused by an increase of the hysteresis loss component in the transverse samples, while the eddy current losses are independent of the cutting arrangement.

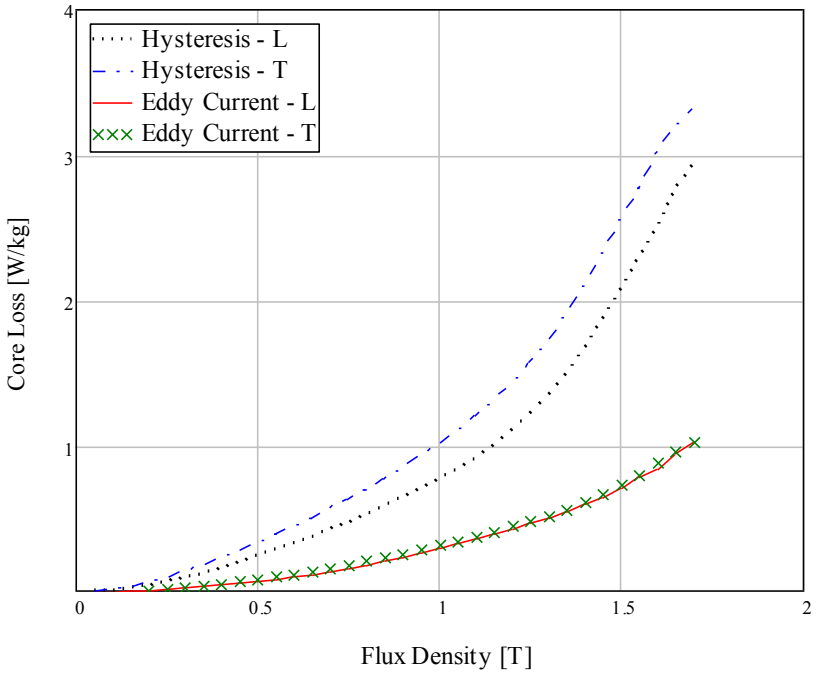

Figure 2.12: Comparison of core loss components in longitudinal (L) and transverse (T) samples measured by the single sheet tester at 60Hz for M19G29.

Core loss results obtained from the two testers for frequencies up to 400Hz are in good agreement, as shown in Fig. 2.13. However, this is not the case in the measured magnetic permeability, shown in Fig. 2.14. The divergence in the measured magnetic

permeability could be caused by miscalculation of the magnetic field strength that is attributed to the accuracy at which the magnetic path length is assumed in both the Epstein frame and the single sheet tester.

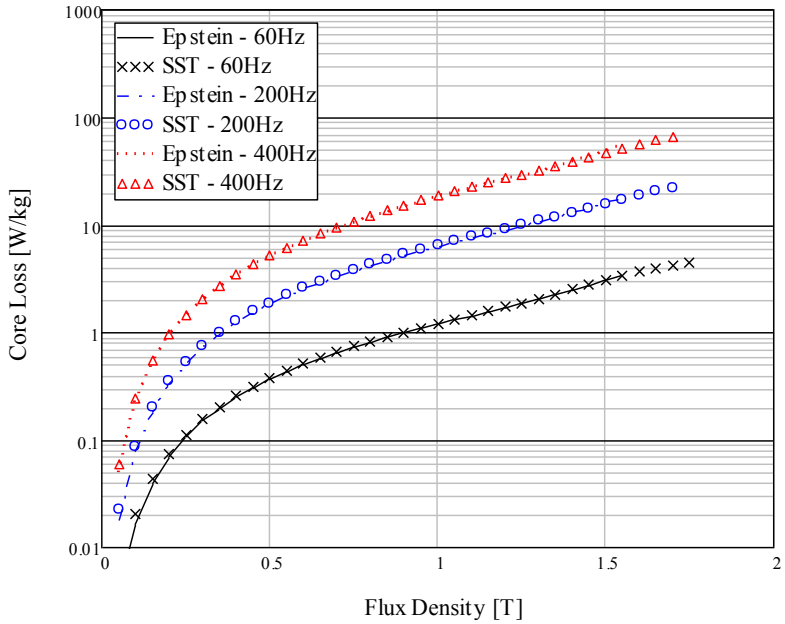

Figure 2.13: Comparison of the core loss measured by the Epstein frame and the single sheet tester for M19G29.

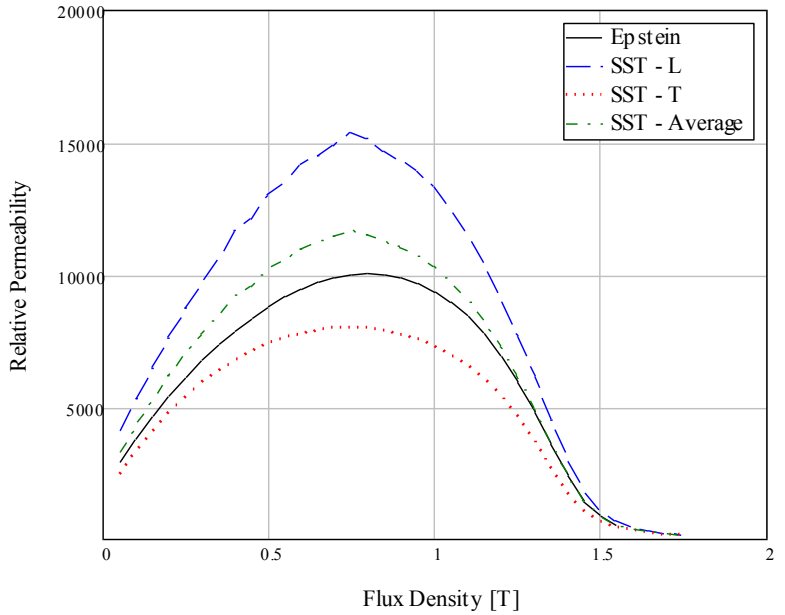

Figure 2.14: Comparison of the magnetic permeability measured by the Epstein frame and single sheet tester for M19G29.

2.6 Summary

Comparative sinusoidal measurements at various frequencies have been performed on the commercial Donart system using the three standardized test fixtures. Discrepancies have been found in the core loss and permeability measured by the Epstein frame and toroid tester with reduced sample size. While the core loss data obtained from the single sheet tester and the Epstein frames are in good agreement, deviations have been found in the measured magnetic permeability by the two test fixtures. In addition to the commercial system, a test bench has been developed to carry out core loss measurements in electrical machine laminations exposed to non-sinusoidal flux.

Chapter 3
Core Loss Separation

This chapter presents a new method for the separation of core loss components (hysteresis and eddy current) in laminations exposed to high frequency excitations. Accurate separation of core losses is achieved by calculating the hysteresis losses at each frequency taking into account the non-uniform flux density distribution inside the lamination. The developed model is then employed to separate the hysteresis and eddy current loss components in annealed and un-annealed laminations. The results are then used to study the effect of the annealing process on core loss components in laminations exposed to high frequency excitations.

3.1 Review of Core Loss Separation Methods

Ideally, the static hysteresis energy loss per cycle is calculated by measuring the area enclosed by the hysteresis loop under static excitation. However, the measurement of the static hysteresis loop requires special instrumentation [21]. When the magnetic material is exposed to a time varying magnetic field, the area enclosed by the measured hysteresis loop represents the total core loss per cycle, which includes both the hysteresis and eddy current loss components. Therefore, an alternative method is usually used to calculate the hysteresis energy loss per cycle using core loss measurements at different frequencies. In this method, the hysteresis loss per cycle is separated by extrapolating core loss per cycle vs. frequency curves at different flux densities to zero frequency. The power loss at zero frequency represents the hysteresis energy loss per cycle. Fig. 3.1 illustrates the separation of core loss components by the extrapolation method.

In the extrapolation method, the hysteresis energy loss per cycle is assumed independent of the frequency, and the total hysteresis loss is simply calculated by multiplying the static hysteresis energy loss per cycle by the operating frequency. This assumption is only valid at low frequencies, where the magnetic field across the lamination is uniform. When the lamination is exposed to a time-varying magnetic field, eddy currents are generated inside the lamination. These eddy currents, according to Lenz's law, produce a secondary magnetic field that opposes the applied field. The eddy current magnetic field is maximum at the center of the lamination, where the contributions of all eddy currents add, and minimum at the lamination surface. The actual magnetic field inside the lamination is the summation of the applied field and the eddy current field. Therefore, the distribution of the actual magnetic field is non-uniform across the lamination thickness, being maximum at the surface and minimum at the center of the lamination. The confinement of the magnetic field around the lamination surface is known as skin effect [22]. At low frequencies, the generated eddy currents are small, and skin effect can be neglected. At high frequencies, skin effect is significant, and the peak flux density differs across the lamination thickness. As a result, the local hysteresis loop and the hysteresis energy loss per cycle vary at each point inside the lamination. This variation affects the total hysteresis energy loss per cycle, making it dependent on the magnetic field distribution, which is strongly affected by the frequency. Therefore, the separation of core loss components by the extrapolation method, assuming constant hysteresis energy loss per cycle, is only valid at low frequencies. When skin effect is significant at high frequencies, accurate core loss separation requires taking skin effect into account in the determination of the core loss components.

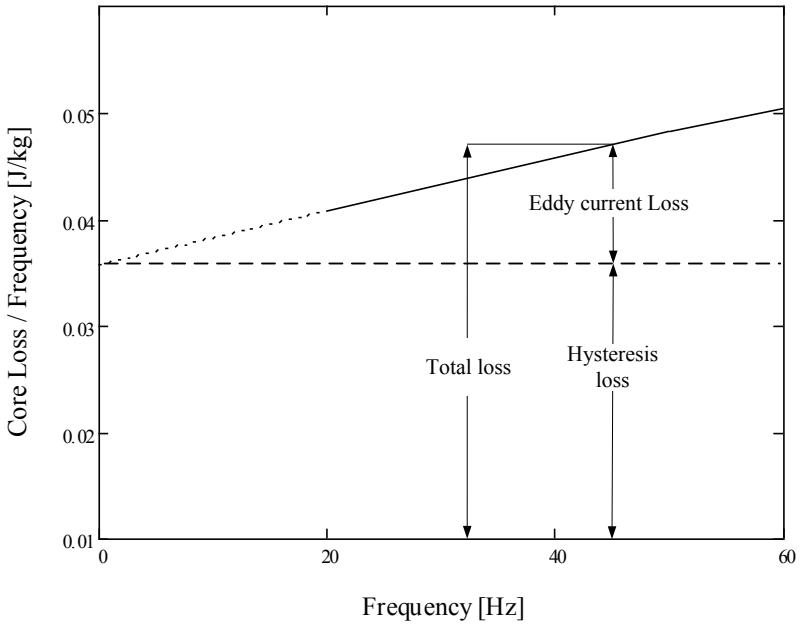

Figure 3.1: Separation of core losses by the extrapolation method.

To achieve an accurate core loss separation, a dynamic finite element model for the non-linear hysteresis loop is adopted [23]. The model was originally developed in [24]. In the model, Maxwell's Equations are solved using the finite element method, where the hysteresis at any location of the material is represented by an energetic hysteresis model [25]. The total losses are assumed to be composed of eddy current and hysteresis losses, which are calculated by the following equations,

$$P_e = \frac{1}{\rho \iiint dtdv} \iiint \frac{\vec{J}_e^2}{\sigma} dvdt \tag{3.1}$$

$$P_h = \frac{1}{\rho \iiint dtdv} \iiint \vec{B} \cdot d\vec{H} dv \tag{3.2}$$

where P_e is the eddy current loss in unit mass and unit time, P_h is the hysteresis loss in unit mass and unit time, ρ is the mass density of the magnetic material , and $\vec{J}_e$ is the

eddy current density in the lamination.

Table 3.1 compares the hysteresis losses calculated by the FE model and the extrapolation method for three different materials. It can be seen that at 50Hz the hysteresis losses obtained from the two methods are in good agreement. While at 1000Hz, the extrapolation method shows large errors in the hysteresis loss determination compared to the FE results for the three materials. At low frequencies, the magnetic field is uniform across the lamination, and the impact of skin effect on the hysteresis losses can be neglected. While at higher frequencies, skin effect is significant. This causes a deviation between the actual and the static hysteresis energy loss per cycle at high frequency. Therefore, it is only justified to use extrapolation at low frequencies.

Accurate separation of core loss components can be achieved by the FE model. However, the long computation time makes it impractical to use for establishing an extensive database of core loss components for various materials at different frequencies and flux densities. Therefore, an alternative method needs to be developed.

Table 3.1: Comparison of hysteresis losses calculated by FE model and extrapolation.

Material	Frequency [Hz]	Extrapolation Loss [W/kg]*	FE Loss [W/kg]*	% Error**
M19 G29	50	0.77	0.80	3.75
	1000	15.37	20.53	25.13
Mill A annealed	50	1.06	1.06	-0.21
	1000	21.23	32.30	34.27
Mill A un-annealed	50	6.02	6.03	0.18
	1000	120.33	136.99	12.16
*At a flux density of 1T. ** Based on the respective FE results.				

3.2 Finite Section Method

This section presents a fast and efficient method for the separation of core losses at high frequencies using an analytical model to describe the flux density distribution across the lamination.

3.2.1 Determination of the Static Hysteresis Loss

The static hysteresis energy loss per cycle is obtained from the measured core losses at two frequencies. These frequencies are chosen so that the influence of skin effect on the core loss components is negligible. When skin effect is negligible, the hysteresis energy loss per cycle is independent of frequency and the total hysteresis losses can be obtained by multiplying the frequency by the static hysteresis energy loss per cycle. Also, the eddy current energy loss can be assumed to change linearly with the frequency. Thus, the total energy loss can be simply represented by,

$$W_t = \alpha_e f + W_h \tag{3.3}$$

W_h , and α_e are the hysteresis energy loss per cycle, and the eddy current loss coefficient. These parameters can be calculated using the measured energy loss data W_1 and W_2 at two frequencies f_1 and f_2, these frequencies should be within a frequency range at which the skin effect is negligible. The static hysteresis energy loss per cycle can be calculated by,

$$W_h = \frac{W_2 f_1 - W_1 f_2}{f_1 - f_2} \tag{3.4}$$

The hysteresis loss formula in (1.1) with constant flux density exponent is found to be only applicable at low flux densities. In order to extend it to higher flux densities, the formula was modified in [5, 26] to,

$$W_h(B) = K_h B^{a+bB+cB^2} \tag{3.5}$$

where K_h, a, b and c are curve fitting constants obtained from the separated hysteresis energy loss per cycle by (3.4) at four values of flux density.

3.2.2 Distribution of Flux Density

In order to study the influence of skin effect on high frequency hysteresis losses, a flux distribution model is adopted. The flux density amplitude at a dimensionless position $\hat{y} = y/L$ from the center of the lamination is given in [22] as,

$$B_p(\hat{y}) = B_b \sqrt{\frac{\cosh(\frac{2\hat{y}}{\lambda}) + \cos(\frac{2\hat{y}}{\lambda})}{\cosh(\frac{2}{\lambda}) + \cos(\frac{2}{\lambda})}} \quad , \tag{3.6}$$

$$\lambda = \sqrt{\frac{2}{L^2 \omega \mu \sigma}} \quad , \tag{3.7}$$

B_b, ω, μ, are the flux density amplitude at the boundary, the angular frequency, and the magnetic permeability, respectively.

The measured parameter in the experiment is the average flux density B_{ave} which deviates from the flux density at the boundary, when skin effect is present. The peak average flux density is given in [10] by,

$$B_{ave} = B_b \lambda \frac{\sqrt{0.5\left[1+\exp\left(\frac{8}{\lambda}\right)\right] - \exp\left(\frac{4}{\lambda}\right)\cos\left(\frac{4}{\lambda}\right)}}{1+2\cos\left(\frac{2}{\lambda}\right)\exp\left(\frac{2}{\lambda}\right)+\exp\left(\frac{4}{\lambda}\right)} \tag{3.8}$$

(3.6) and (3.8) are obtained from the solution of Maxwell's equation with an assumption of a linear magnetic material. However, the distribution of flux density is dependent on the magnetic permeability which varies along the hysteresis curve depending on the flux density level. The variation of magnetic permeability affects the distribution of flux density across the lamination thickness, being non-uniform for high values of magnetic permeability and more uniform for low values of permeability at low fields and near saturation. To account for the variation of field distribution with the flux density level, the magnetic permeability is allowed to vary with the flux density. Therefore, the permeability is expressed as a 4th order polynomial,

$$\mu(B) = K_0 + K_1(B_{ave}) + K_2(B_{ave})^2 + K_3(B_{ave})^3 + K_4(B_{ave})^4 \tag{3.9}$$

where K_0 to K_4 are curve fitting coefficients obtained from the measured magnetic permeability at low frequency. Using (3.6-3.9), the distribution of flux density across the lamination at a certain measured average flux density can be calculated, knowing the operating frequency and the properties of the lamination.

In order to validate the analytical flux model, its results are compared with the flux waveforms obtained from the FE model. The results, in Fig. 3.2, show good correlation between the flux waveforms obtained from the two models at different

locations inside the lamination. This means that the analytical flux model can calculate the peak flux density across the lamination thickness, and therefore can be used to determine the local hysteresis loops.

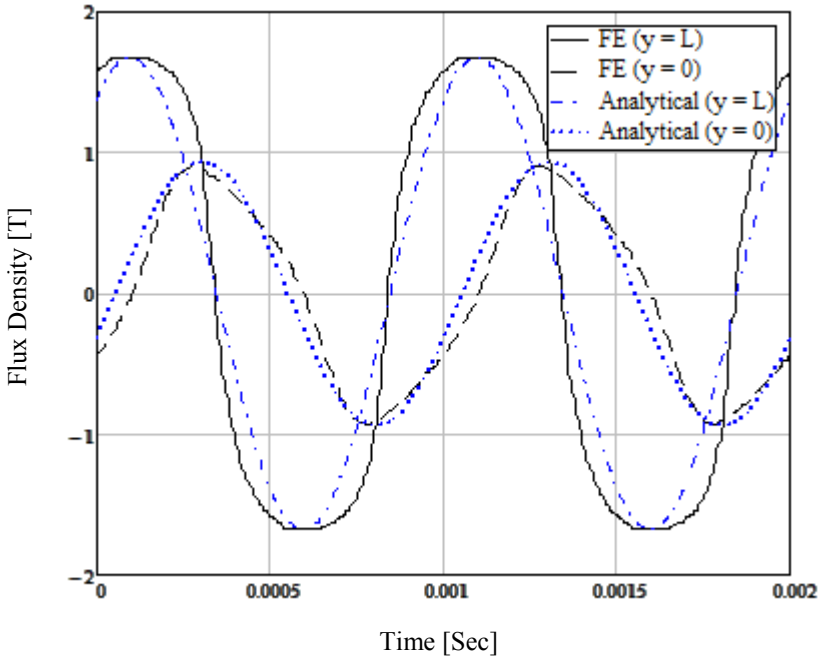

Figure 3.2: Comparison of FE and analytical flux density waveforms at different locations for un-annealed laminations at 1000Hz.

When skin effect is significant, the value of the measured average flux density is no longer an accurate measure of the actual flux density inside the lamination which differs in magnitude at each point across the lamination thickness. In addition to the magnitude variation caused by skin effect, there is also a phase difference in the flux density waveforms at different points across the lamination. This time delay causes the peak flux density at different points to occur at different instants of time, and therefore the measured average flux density is not necessarily the average value of these peak flux densities. For all the above mentioned cases, the actual hysteresis energy loss per cycle at

high frequency is no longer equal to the static hysteresis energy loss per cycle at a certain measured average flux density. Therefore, accurate quantification of hysteresis losses at high frequency requires considering the realistic flux distribution inside the lamination.

3.2.2 Model Description

A model is implemented to achieve accurate quantification of high frequency hysteresis losses, taking into account the realistic flux distribution. The calculation starts with constructing the flux density distribution across the lamination thickness using (3.6-3.9). The lamination is then divided into n sections. At each section, the hysteresis energy loss per cycle is calculated from (3.5), depending on the value of the peak flux density. The total hysteresis loss is then calculated by summing the power loss of all the sections. Fig. 3.3 illustrates the variation of hysteresis loops across the lamination thickness. A flow chart of the model is shown in Fig. 3.4.

The model results, displayed in Fig. 3.5, show that the hysteresis energy loss per cycle increases at high frequencies, especially when skin effect is significant at high values of magnetic permeability. While at low fields and near saturation, the hysteresis energy loss per cycle is almost equal to its values at low frequencies. This variation affects the hysteresis loss curve, making it more linear at high frequencies. This implies that the flux density exponent in the original Steinmetz equation should be a function of the frequency, as well as the flux density.

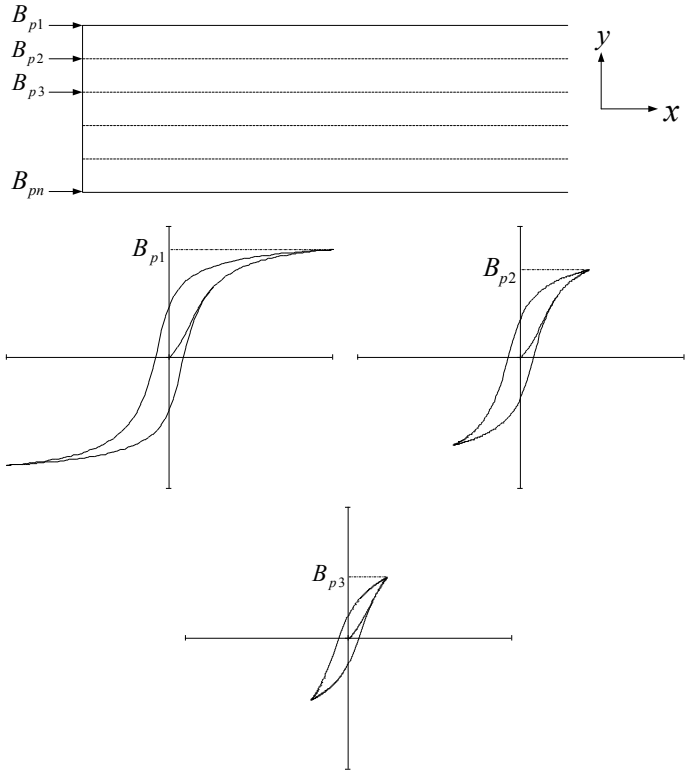

Figure 3.3: Illustration of the variation of hysteresis loops across the lamination.

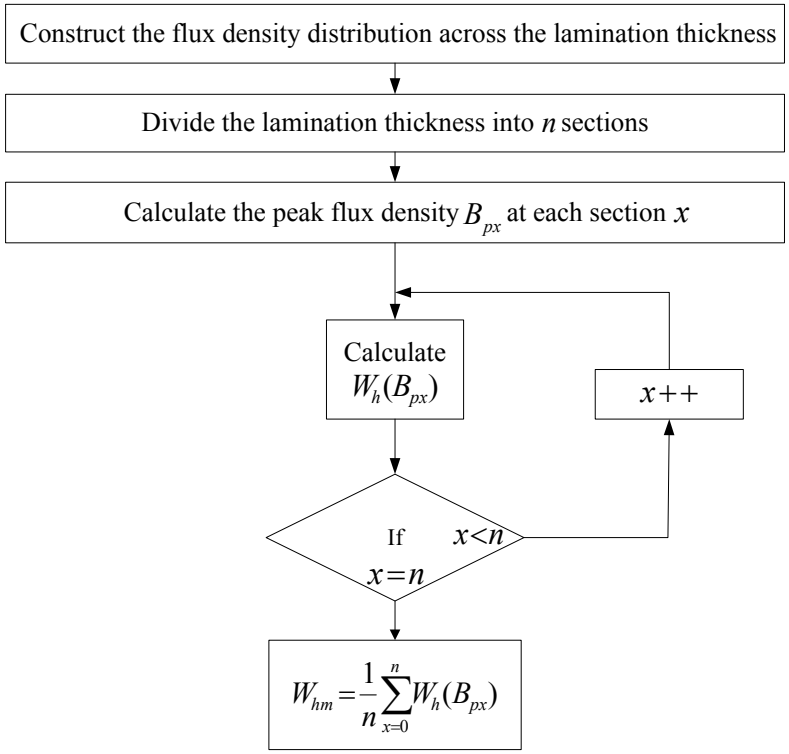

Figure 3.4: Flow chart of the model.

The model results are compared with the hysteresis losses calculated by the FE model and the extrapolation method. Table 3.2 compares the hysteresis losses obtained by the three methods at different frequencies of 1T and 1.5T for un-annealed laminations. It can be seen that the model results are in good agreement with the FE hysteresis losses at all the tested frequencies up to 2000Hz. In addition, at low frequency, when skin effect is negligible, the extrapolation method shows good accuracy compared to the model and FE results. At high frequency, the hysteresis losses calculated the extrapolation method shows large errors up to 17.65% at 2000Hz and 1T compared to the model results. Also, it is clear from Table 3.2 that the variation of the hysteresis energy loss per cycle with frequency is more severe at 1T than at 1.5T where the magnetic field distribution is more uniform.

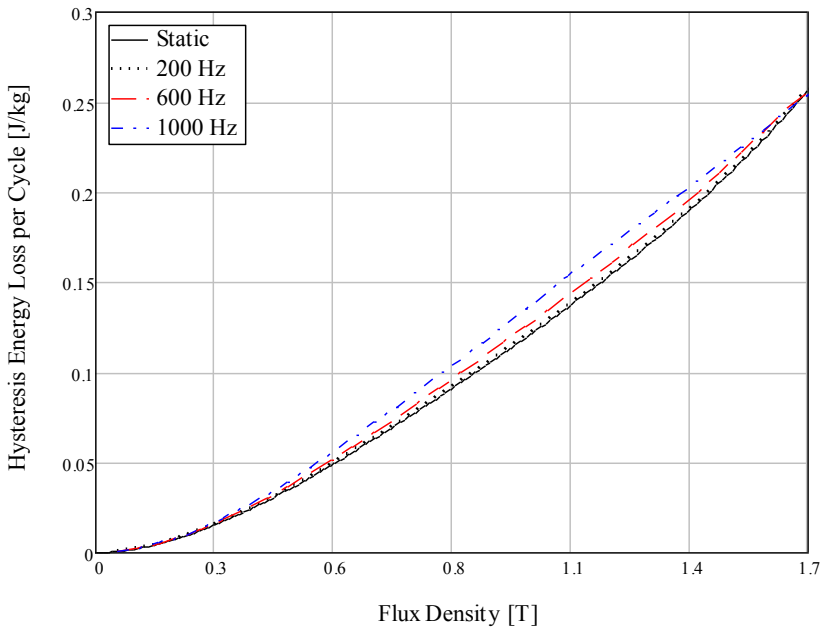

Figure 3.5: Model result for un-annealed laminations.

Table 3.2: Comparison of hysteresis losses calculated by different separation methods.

Frequency [Hz]	Flux Density [T]	FE Loss [W/kg]	Extrapolation Loss [W/kg]	% Error *	Model Loss [W/kg]	% Error *
50	1.00	6.03	6.02	0.18	6.00	0.41
	1.50	10.93	10.90	0.32	10.90	0.33
200	1.00	24.60	24.07	2.18	24.16	1.79
	1.50	44.04	43.60	1.00	43.70	0.76
600	1.00	76.35	72.20	5.45	75.98	0.49
	1.50	133.09	130.80	1.72	133.91	-0.61
1000	1.00	136.99	120.33	12.16	136.50	0.36
	1.50	222.31	218.00	1.94	226.14	-1.72
2000	1.00	313.46	240.65	23.23	292.22	6.77
* Based on the respective FE results.						

3.3 Effect of Annealing on Core Loss Components

The finite section method is used to separate the measured core losses in annealed and un-annealed laminations into hysteresis and eddy current loss. The separated losses are then used to analyze the effect of annealing on core loss components in laminations exposed to high frequency excitations.

3.3.1 Total Loss

Comparative core loss measurements are performed on dry, wet annealed and un-annealed laminations with 0.61mm thickness at various frequencies in the range of 20Hz – 4000Hz. Fig. 3.6 shows that the particular annealing process (wet or dry) does not affect the total core loss measured at different frequencies.

Table 3.3 shows a comparison of the measured core loss in the annealed and un-annealed samples at different frequencies. From Table 3.3, it is clear that a significant reduction in the low frequency core loss is achieved by annealing. This reduction decreases with raising the frequency, until the effect of annealing on the total core loss

can be neglected at high frequencies and high densities, as shown in the measured core loss in Fig. 3.7. In addition, the magnetic properties of the material are recovered by annealing. This can be clearly observed in the measured magnetic permeability, shown in Fig. 3.8.

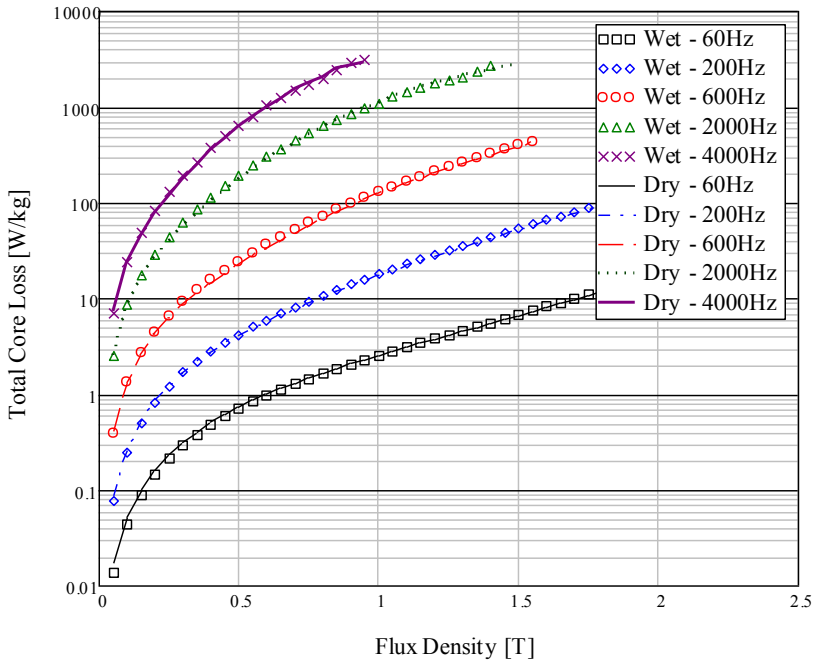

Figure 3.6: Effect of the particular annealing process on the measured total core loss.

Table 3.3: Core loss reduction by annealing.

Frequency [Hz]	Flux Density [T]	Un-annealed Losses [W/kg]	Annealed Losses [W/kg]	%Difference*
20	1	2.4531	0.5487	77.63
50	1	6.734	1.9778	70.62
60	1	8.4422	2.5647	69.62
200	1	38.299	18.188	52.5
600	1	193.3	130.14	32.67
1000	1	424.11	323.54	23.71
2000	1	1211.5	1104.9	8.80
4000	0.85	2508.6	2424	3.37
* Based on the respective un-annealed losses.				

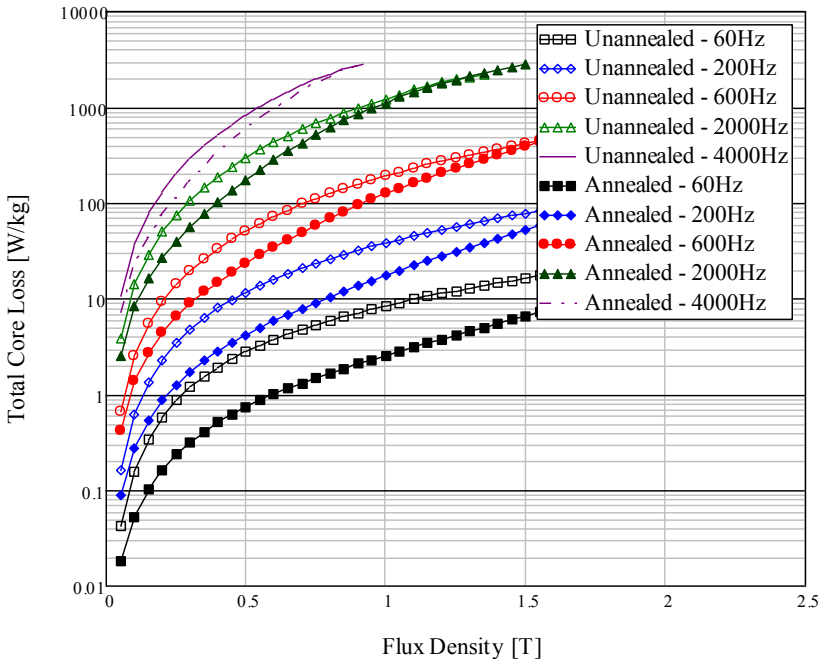

Figure 3.7: Effect of annealing on the measured total core loss.

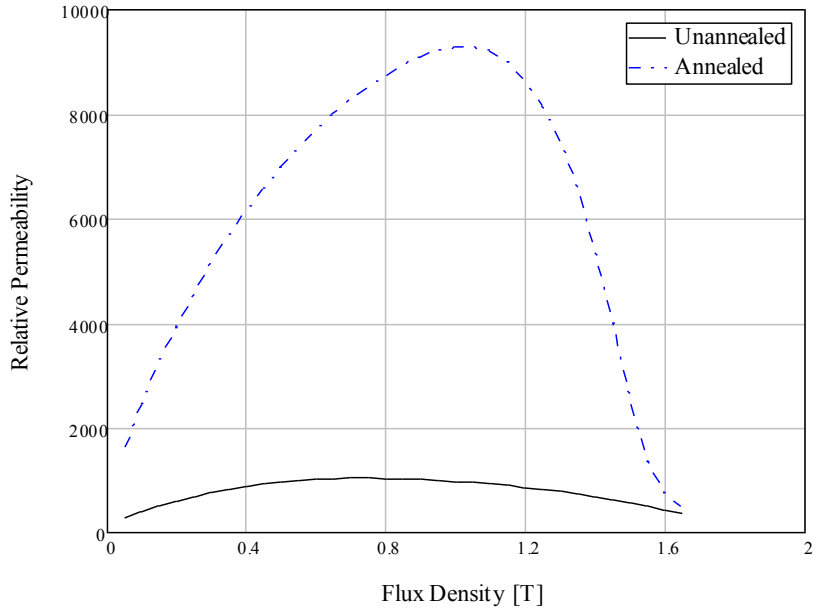

Figure 3.8: Effect of annealing on the magnetic permeability measured at 20 Hz.

3.3.2 Hysteresis Loss

The reduction in the total core loss at low frequency achieved by annealing is mainly attributed to the reduction in the hysteresis loss component, shown in Fig. 3.9.The reduction in the hysteresis loss by annealing was also reported in [16, 20]. The hysteresis loss is the dominant loss component at low frequencies. This can be seen from the ratio of hysteresis to eddy current at different frequencies in Fig. 3.10. At high frequency, the reduction in the hysteresis losses has less impact on high frequency core losses, as the eddy current loss forms the larger portion of the total core losses. Moreover, the hysteresis energy loss per cycle increases at high frequency due to skin effect. Since the magnetic field distribution in steels with high permeability tends to be non-uniform, the hysteresis loss is more likely to be influenced by skin effect in the annealed samples.

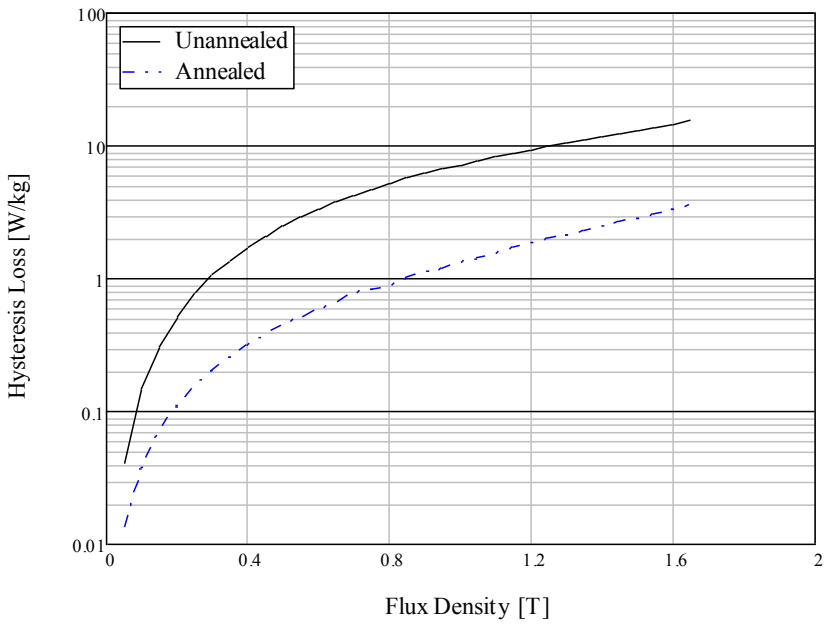

Figure 3.9: Effect of annealing on the hysteresis loss at 60 Hz.

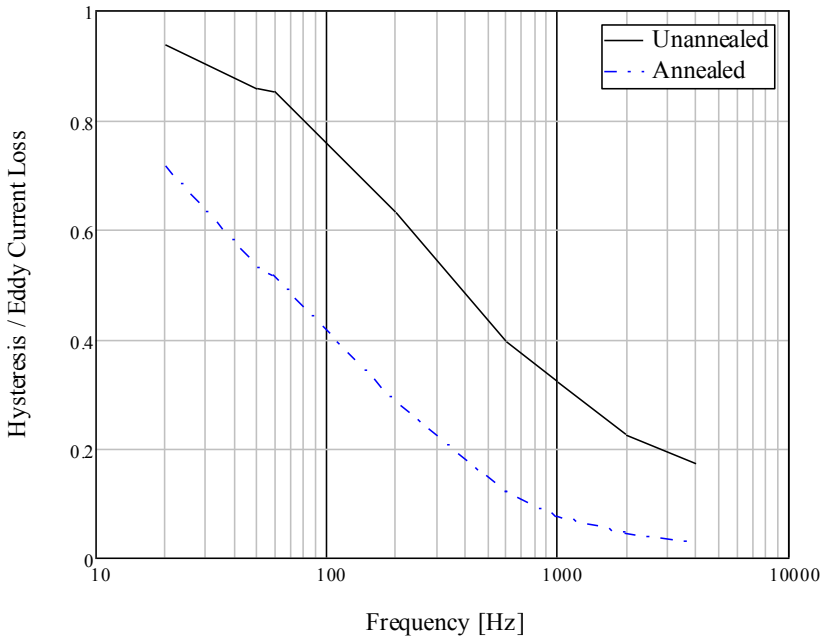

Figure 3.10: Ratio of hysteresis to eddy current losses at different frequencies.

3.3.3 Eddy Current Loss

While the annealing process is beneficial in terms of reducing the hysteresis loss and improving the magnetic properties of the material, it causes an increase in the eddy current loss. Fig. 3.11 shows the effect of annealing on eddy current loss at 1T and 1.5T. It can be observed that the eddy current loss at 1T is less affected by annealing for frequencies lower than 1000 Hz. For higher frequencies, the eddy current loss is higher in the annealed samples. At 1.5T, the annealing increases the eddy current loss at all the tested frequencies.

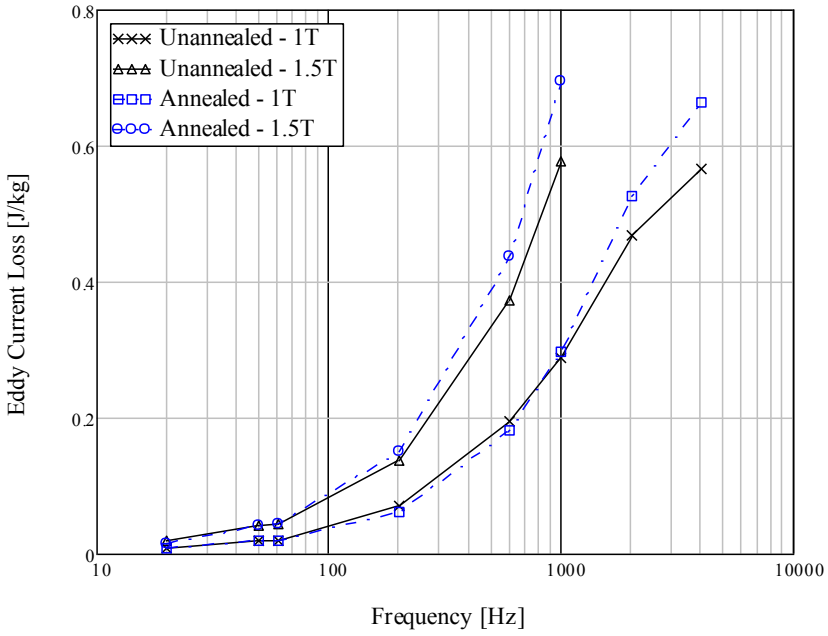

Figure 3.11: Effect of annealing on the eddy current loss.

In order to study the effect of annealing on eddy current loss, the measured eddy current loss is compared with the results obtained from an analytical eddy current loss formula that accounts for the non-uniform distribution of magnetic field at high frequency. The eddy current loss is represented in [4] by,

$$P_e = \frac{\omega B_{av}^2}{2\lambda\mu\rho} \frac{\left[\exp\left(\frac{4}{\lambda}\right) + 2\cos\left(\frac{2}{\lambda}\right)\exp\left(\frac{2}{\lambda}\right) + 1\right]\left[\exp\left(\frac{4}{\lambda}\right) - 2\exp\left(\frac{2}{\lambda}\right)\sin\left(\frac{2}{\lambda}\right) - 1\right]}{\left[1 - 2\exp\left(\frac{4}{\lambda}\right)\cos\left(\frac{4}{\lambda}\right) + \exp\left(\frac{8}{\lambda}\right)\right]} \tag{3.10}$$

As shown in Fig. 3.12, the formula predicts eddy current loss in the un-annealed sample accurately, while a significant deviation is found between the predicted and calculated eddy current loss in the annealed samples, where the eddy current loss is

underestimated substantially. The formula is based on the solution of Maxwell's equations with an assumption of linear magnetic material. According to this assumption, the eddy current loss should be reduced in the annealed samples, where skin effect is more significant due to its high magnetic permeability, as illustrated in Fig. 3.13, this forces the eddy currents to flow in a smaller area, increasing the resistance of the eddy current path and limiting the induced eddy currents, and thus reducing the eddy current losses, as shown in the calculated loss in Fig. 3.14. In contrast, the measured eddy current loss in the annealed samples is much higher than the predicted values and even higher than the eddy current loss in the un-annealed samples.

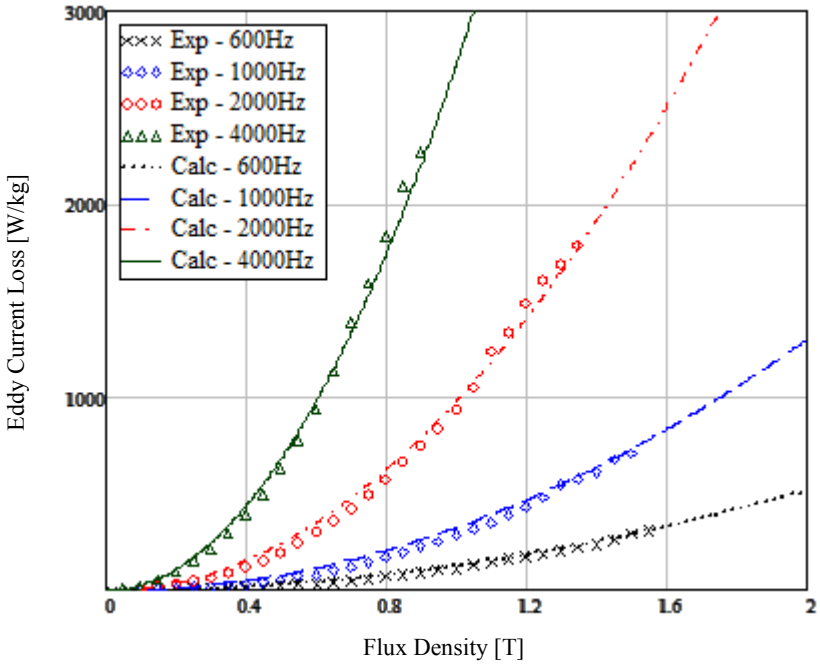

Figure 3.12: Comparison between calculated and measured eddy current loss in the un-annealed laminations.

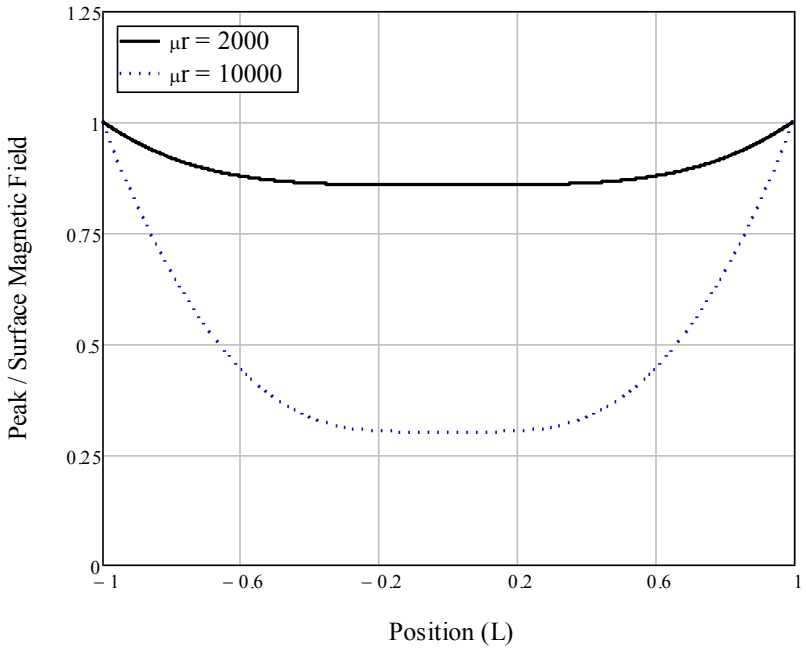

Figure 3.13: Effect of the permeability on magnetic field distribution at 200 Hz.

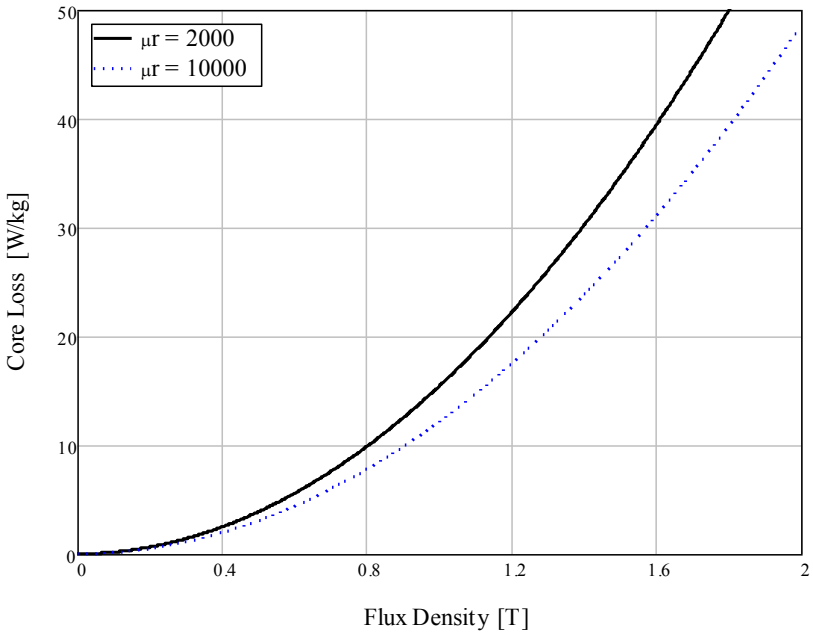

Figure 3.14: Calculated eddy current loss for different values of magnetic permeability at 200Hz.

The annealing process changes the magnetic properties of the material. This can be clearly seen in the measured hysteresis loops before and after annealing, shown in Fig. 3.15 and 3.16, respectively. Below the knee of the lower branch of the hysteresis curve for annealed samples, it is clear that a small change in the magnetic field causes a large increase in the flux density. While beyond the knee, the flux density variation is small corresponding to large changes in the magnetic field. This distinctive shape of the hysteresis loop in the annealed samples causes the local flux density to follow almost rectangular profiles. The steep edges of the local flux density waveforms increase the eddy current loss in the annealed samples, especially at high flux densities, where the rectangular profiles of flux density are more pronounced. Therefore, the assumption of constant magnetic permeability is not able to represent the magnetic behavior of the annealed laminations. Moreover, the annealing process causes the grain size of the magnetic material to increase. Growing larger grains is associated with the existence of more widely spaced domain walls, which means that the individual walls have to move faster to produce certain flux change. The rapid movement of walls increases the eddy current loss as the eddy currents are located at the moving domain walls [27]. The effect of domain structure on eddy current loss can be neglected in the un-annealed samples, as it has fine domain structure [28].

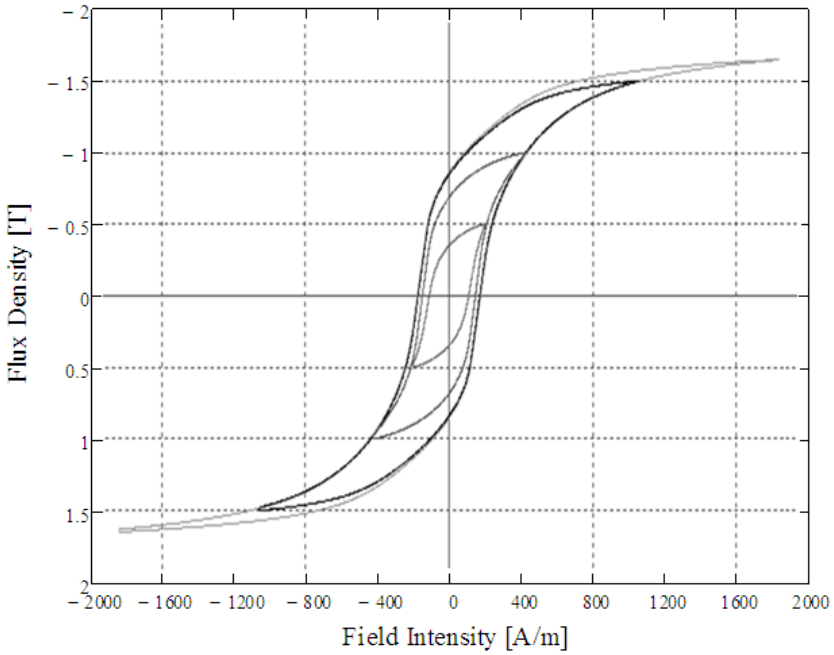

Figure 3.15: Measured hysteresis loops in the un-annealed laminations at 20Hz.

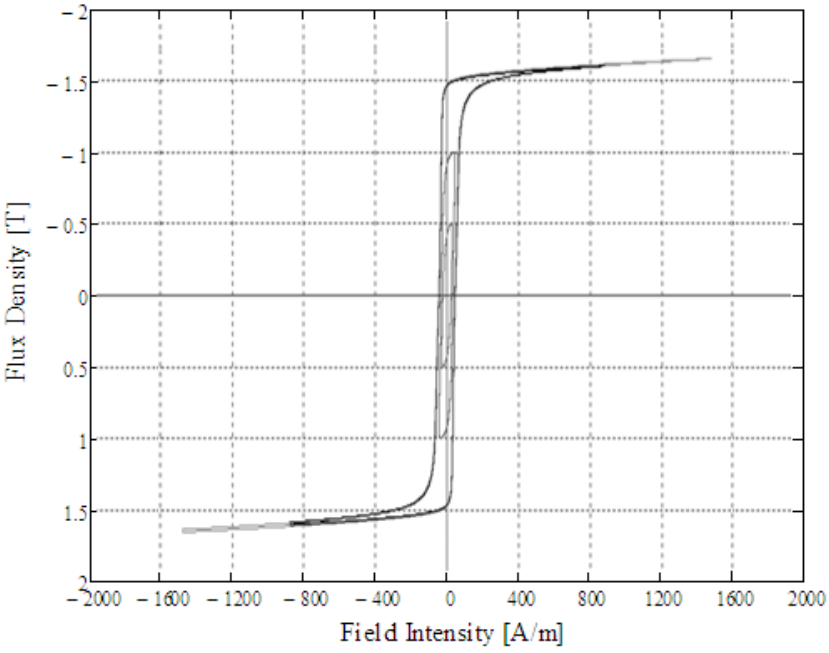

Figure 3.16: Measured hysteresis loops in the annealed laminations at 20Hz.

3.4 Summary

A model has been implemented to calculate the hysteresis losses taking into account the non-uniform flux distribution. The results show that the assumption of constant hysteresis energy loss per cycle is only valid at low frequencies where skin effect is negligible. While at high frequency, the flux density amplitude varies at each point inside the lamination. As a result, the hysteresis energy loss per cycle increases, and tends to change linearly related to the flux density.

Comparative core loss measurements have been performed on annealed and un-annealed samples at various frequencies up to 4000Hz. Accurate separation of core loss components is achieved by using the developed separation model. The annealing process is found to decrease the hysteresis losses, while the eddy current losses are higher in the annealed samples, especially at high frequencies and high flux densities.

Chapter 4

Prediction of Core Losses under Non-sinusoidal Flux

4.1 Core Loss Modeling

Most of the available core loss models in electrical machine design software are based on the assumption of uniform magnetic field distribution inside the lamination [3, 4]. However, this assumption is not valid in the laminations exposed to high frequency excitations, where skin effect is pronounced. The conventional core loss models can be extended to higher frequencies by using variable core loss coefficients, which are extracted from the measured core losses [5]. The ranges of frequency and flux density, at which accurate core loss prediction can be achieved, are dependent on the available core loss data under sinusoidal excitations. However, the actual flux waveforms inside many machines, e.g., permanent magnet (PM) machines and switched reluctance (SR) machines are non-sinusoidal and differ in different parts of the machine. In addition, the flux distortion can be caused by the distorted supplies, e.g., pulse width modulation (PWM) inverter fed induction machines. Since, there is an infinite number of possible flux waveforms in electrical machines, it is impractical to depend on the non-sinusoidal core loss measurements in the determination of the core loss under distorted flux. Due to the non-linear nature of the core loss mechanism, the estimation of core loss by curve fitting that use the sinusoidal core loss data can cause errors in the core loss estimation when the flux waveforms are distorted. Therefore, the calculation of core losses in laminations exposed to non-sinusoidal flux should be performed using a physics based core loss model that is derived from the physical characteristics of the core loss mechanism in

magnetic materials, and can describe the non-linear nature of core losses under any distorted flux.

This chapter presents a physics based core loss model for the determination of core losses in laminations exposed to non-sinusoidal flux, taking into account the non-uniform distribution of the magnetic field inside the lamination. The results are verified experimentally by comparing to the measured losses in laminations exposed to the flux that exist in different sections of SR and PM machines.

4.1.1 Eddy Current Loss Modeling

Eddy currents are induced in the laminations when it is exposed to a time varying magnetic field; these currents produce a secondary magnetic field that opposes the applied field. The eddy current magnetic field causes the total magnetic field to become non-uniform across the lamination thickness, as the field magnitude at the lamination surface is higher than its magnitude at the center of the lamination. This phenomenon (skin effect) is pronounced when the lamination is exposed to high frequency excitations, especially for thicker laminations. The confinement of the magnetic field to the lamination surface changes the effective resistance of the eddy current path, as the eddy currents circulate through a smaller area, which increases the resistance of the eddy current path, and therefore decreases the eddy current losses in the lamination. This explains why the classical eddy current loss formula that assumes a uniform magnetic field distribution overestimates the eddy current losses, when the laminations are exposed to high frequency magnetic field.

The magnetic field distribution can be obtained analytically from the solution of Maxwell's equations with an assumption of constant magnetic permeability μ [10]. In a

lamination exposed to a sinusoidal surface magnetic field with an amplitude H_0, the magnetic field H in a dimensionless position $\hat{y}$, at a time t can be obtained by,

$$H(\hat{y},t) = H_0 \exp\left(\frac{1-\hat{y}}{\lambda}\right) \times [1 + 2\cos(\frac{2}{\lambda})\exp(\frac{2}{\lambda}) + \exp(\frac{4}{\lambda})]^{-1}$$
$$\times \left[\begin{array}{l} \cos\left(\omega t + \frac{1-\hat{y}}{\lambda} - \right) + \exp\left(\frac{2}{\lambda}\right)\cos\left(-\omega t + \frac{1+\hat{y}}{\lambda}\right) \\ + \exp\left(\frac{2\hat{y}}{\lambda}\right)\cos\left(\omega t + \frac{1+\hat{y}}{\lambda}\right) + \exp\left(\frac{2y+2}{\lambda}\right)\cos\left(\omega t + \frac{-1+\hat{y}}{\lambda}\right) \end{array} \right] \quad (4.1)$$

Many analytical models are presented in the literature to calculate the eddy current loss in electrical machine laminations taking into account the non-uniform magnetic field distribution inside the lamination. The eddy current losses calculated using the material properties and the lamination dimensions are much lower than the total measured eddy current losses. The difference is usually compensated by extracting the coefficient from the experimental data [29], or by using variable core loss coefficients that requires using high frequency core loss measurements [26]. The main reason for this divergence stems from the fact that the developed formulas express the eddy current loss as a function of the peak flux density at the boundary B_b, and the calculated losses are compared to the measured eddy current loss at a certain measured peak flux density. However, the measured flux density in the experiment represents the average flux density over the lamination, which deviates from the flux density at the boundary when the skin effect is significant [10]. The peak average flux density over the lamination can be calculated by (3.8), and the eddy current losses at certain measured peak average flux density can be represented by (3.10).

In order to ensure that the skin effect is pronounced, the calculated loss by (3.10) is compared to the measured eddy current loss in fully processed M19G24 laminations at 400 Hz. It is observed that the eddy current loss calculated by (3.10) underestimates the loss, especially at high flux densities. This divergence is mainly attributed to the assumption of constant magnetic permeability. This assumption means that the flux density at any position in the lamination is linearly related to the field intensity. While this assumption allows an analytical solution of Maxwell's equation, the actual magnetic permeability in the lamination is not constant. The variation of the magnetic permeability is summarized below,

1. The permeability is dependent on the position inside the lamination. Fig. 4.1 shows the flux density variation in time for M19G24 at 400Hz. It can be seen that, due to skin effect, the flux density waveforms differ in magnitude and phase along the lamination thickness. This causes different hysteresis loops to occur at different points inside the lamination. With the differential permeability defined as the local slope of the hysteresis loop, the permeability is changing along the lamination thickness with the variation of the hysteresis loops.

2. At a certain position inside the lamination, the differential permeability is also changing in time, as the local slope of the hysteresis loop is varying during the electrical cycle of the local magnetic field, being maximum at coercivity, and decreasing towards the tip of the local hysteresis loop.

3. The permeability is also affected by the value of the peak measured average flux density, as the local hysteresis loop wave shapes is strongly dependent on the flux density level.

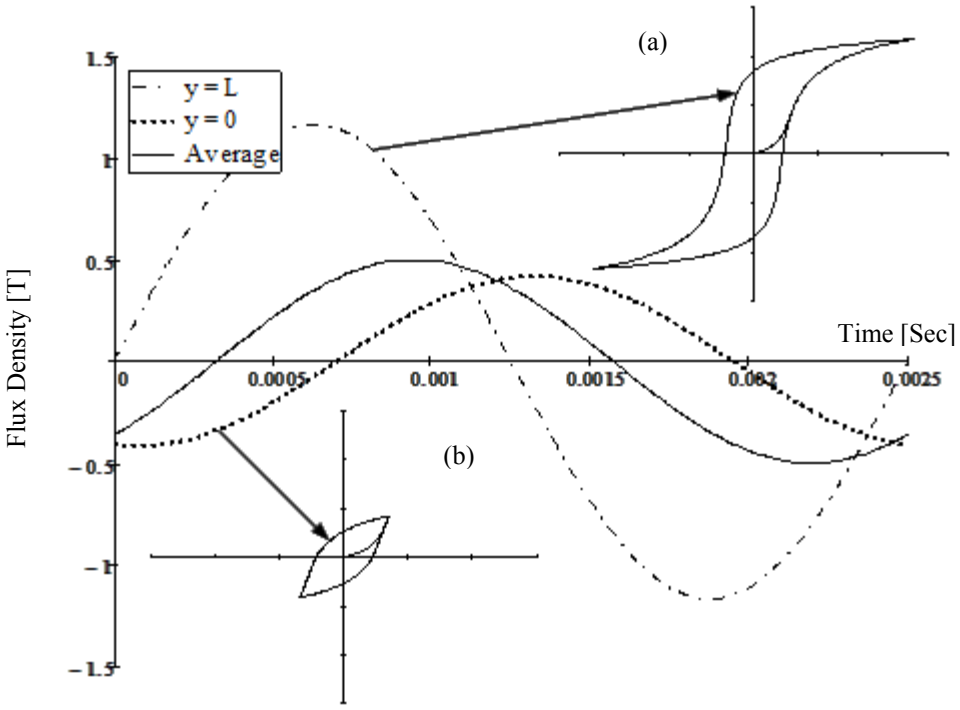

Firure 4.1: Illustration of flux density variation in time and space for M19G24 at 400Hz, with (a) and (b) being the simulated hysteresis loops at the surface and center of the lamination, respectively.

The choice of the effective magnetic permeability is a critical factor in the determination of the eddy current losses, as its value controls the magnetic field distribution inside the lamination. It is observed that the skin effect increases for higher values of permeability. The decrease in the effective area of the magnetic field due to a higher permeability increases the resistance of the eddy currents path, and decreases the eddy current loss calculated by (3.10) for the same peak average flux density. Higher losses are reported in [10] by choosing the effective permeability according to the value of the magnetic field at the boundary. The calculated losses are higher than the measurements because the value of magnetic permeability substituted in Maxwell's equation describes the relationship between the flux density and the field intensity at any position in the lamination. At higher frequencies, the magnetic field inside the lamination

is much lower than the field at the boundary, due to skin effect. Therefore, the magnetic permeability chosen according to the field at the boundary does not reflect the permeability variation inside the lamination, hence the overestimation of the eddy current loss.

In order to account for the variation of the magnetic permeability through the lamination, the permeability is chosen according to the average flux density through the lamination, this parameter can be easily obtained from experiment. The magnetic permeability variation in time is approximated by considering the slope of the line from the origin of the hysteresis loop to the peak flux density. The permeability that represents the material magnetic behavior is obtained from low frequency measurements, where the magnetic field is uniform through the lamination. This permeability is expressed as a function of the peak average flux density B_{av} with a 4th order polynomial. Therefore, λ is modified to,

$$\lambda(B_{av}) = \sqrt{\frac{2}{L^2 \omega \sigma \mu(B_{av})}}, \tag{4.2}$$

and the eddy current loss is expressed as,

$$\begin{aligned} P_{evp} = {} & \frac{\omega K_E B_{av}^2}{2\lambda\mu\rho}\left[1-2\exp\left(\frac{4}{\lambda(B_{av})}\right)\cos\left(\frac{4}{\lambda(B_{av})}\right)+\exp\left(\frac{8}{\lambda(B_{av})}\right)\right]^{-1} \\ & \times\left[\exp\left(\frac{4}{\lambda(B_{av})}\right)+2\exp\left(\frac{2}{\lambda(B_{av})}\right)\cos\left(\frac{2}{\lambda(B_{av})}\right)+1\right] \\ & \times\left[\exp\left(\frac{4}{\lambda(B_{av})}\right)-2\exp\left(\frac{2}{\lambda(B_{av})}\right)\sin\left(\frac{2}{\lambda(B_{av})}\right)-1\right] \end{aligned} \tag{4.3}$$

where K_E is a factor derived from the Pry and Bean model that accounts for the concentration of the eddy currents around the domain walls [27]. While the original model was derived based on a simple domain structure that does not consider the domain

wall bowing at high frequencies, the eddy current loss calculated by (4.3) surprisingly shows good correlation with the measured eddy current losses over a wide range of frequencies up to 2000 Hz for M19G29. Fig. 4.2 shows a comparison between the results of different eddy current loss formulas compared to the measured losses. It is clear that the developed model predicts accurately the eddy current losses, unlike the classical formula P_{cl} that overestimates the losses at high frequency and the loss formula P_e with a constant permeability, extracted from the low flux region of the hysteresis curve, which underestimates the eddy current loss.

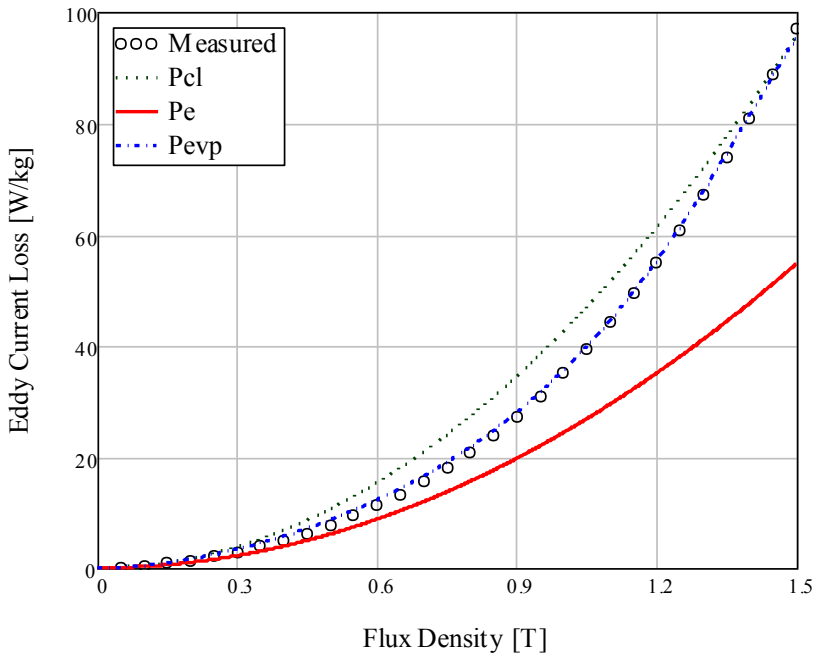

Firure 4.2: Comparison of different eddy current loss formulas with the measured losses for M19G24 at 400Hz.

For any particular flux waveform with a fundamental frequency f_1, the flux density is decomposed into a Fourier series of harmonics. The contribution of each component into the eddy current loss is calculated based on the magnitude of the harmonic, and the harmonic frequency which determines the flux penetration of the

individual harmonics. The total eddy current loss is then calculated from,

$$P_{eT} = \sum_{i=1}^{N} P_{evp}(B_i, if_1) \tag{4.4}$$

4.1.1 Hysteresis Loss Modeling

The hysteresis energy loss is generally assumed independent of the flux rate of change. However, this assumption is not accurate when the skin effect is pronounced at higher frequencies. The skin effect causes the magnetic field distribution to be non-uniform through the lamination, therefore the peak flux density varies in different parts of the lamination, this causes local hysteresis loops, and therefore the local hysteresis energy loss per cycle to differ at different points inside the lamination. The hysteresis loss at high frequencies can be calculated by constructing the magnetic field distribution across the lamination. However this procedure is computationally expensive, especially when the flux density waveform is non-sinusoidal, as it becomes difficult to obtain the flux density distribution using analytical models. Therefore, this method is not suitable for core loss determination in finite element (FE) machine design software, which requires fast core loss calculation at each mesh element. Therefore, the total hysteresis energy loss is assumed to be only dependent on the flux density amplitude, wave shape, and the fundamental frequency. The total hysteresis loss is calculated by the addition of the hysteresis losses due to major and minor hysteresis loops using,

$$P_{hT} = f_1 K_h \hat{B}^{a+b\hat{B}+c\hat{B}^2} \left(1 + \frac{0.65}{\hat{B}} \sum_{i=1}^{n} \Delta B_i\right) \tag{4.5}$$

where n is the number of minor hysteresis loops per half cycle, and ΔB is the magnitude of the minor loop [30]. The coefficients K_h, a, b and c can be obtained from the

separated hysteresis loss by (2.1).

4.2 Core Losses in Permanent Magnet (PM) Machines

In PM machines the ratio of iron to copper losses is high, thus a potential improvement in the machine efficiency can be achieved by reducing the core losses with an optimized machine design [16]. In addition, the prediction of PM machine temperature is essential, since the temperature rise affects the flux density of the permanent magnets, and therefore the machine output torque capability [31]. Prediction of machine temperature requires considering all sources of power loss. One of these heat sources is the core loss. The difficulty of core loss prediction in PM machines is caused by the flux distortion in the machine core, as the flux waveforms differ in different parts of the machine, and they also vary with the machine loading condition.

The machine under consideration is a 4 pole 24 slot PM machine with inset permanent magnets for the additional reluctance torque. The machine was originally designed in [32] for use as a traction motor in a lift truck application.

4.2.1 Flux Waveforms

The flux waveforms in different sections of the machine are obtained using MagneForce FE software. These waveforms are generated in the laminations using the test bench, and the specific core losses in various sections of the machine core are measured.

In order to calculate the flux density variation in the machine core, the finite element simulation is performed for several rotor positions in order to construct the flux density waveforms during one electrical cycle. The flux density waveforms are obtained

when the machine is operating at no-load and under loading conditions. Fig. 4.3 and 4.4 show the flux distribution of the inset PM machine at no-load and full load, respectively.

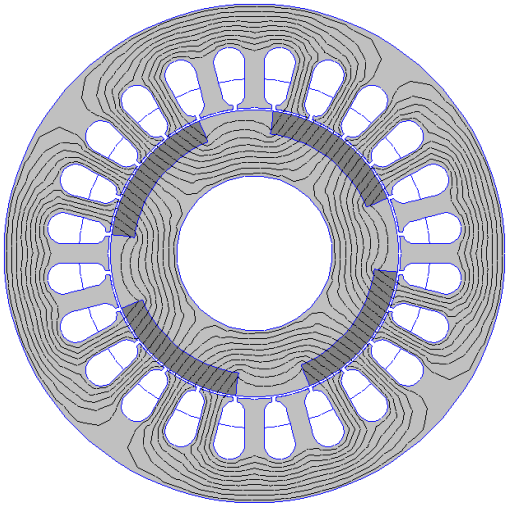

Firure 4.3: Flux distribution of the inset PM machine at no-load.

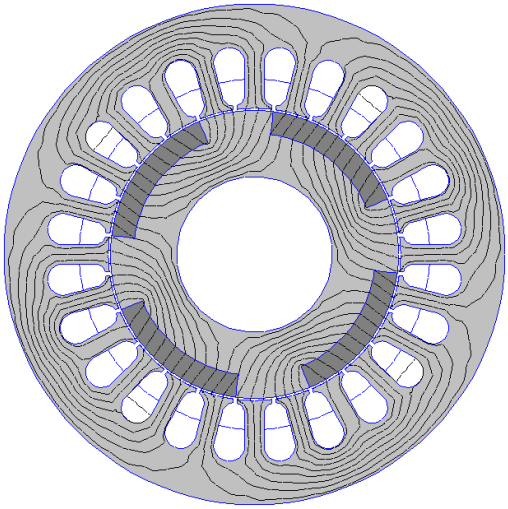

Firure 4.4: Flux distribution of the inset PM machine at full-load.

The flux density magnitude in a certain mesh element is obtained from the two orthogonal components B_x and B_y from,

$$|B| = \sqrt{B_x^2 + B_y^2} \tag{4.6}$$

Fig. 4.5 shows the flux density variation in the middle of the stator tooth when the machine is operating at no-load. Since there is no armature flux, the flux waveforms in the machine core is only attributed to the rotation of the magnets, the flux density in the stator tooth rises linearly when the rotor magnet leading edge passes by the stator tooth, and it remains almost constant, while the tooth is fully covered by the magnet. When the magnet trailing edge passes by the tooth, the flux density decreases linearly until it reaches zero and it remains constant until the leading edge of the next magnet begins to pass by the tooth [31, 33]. Fig. 4.6 shows the flux density variation in the stator yoke. The flux density waveform follows approximately a trapezoidal function, as the flux density rises linearly from the negative plateau to the positive plateau when the magnet traverses the considered point [31, 33]. The flux variation in the rotor can be neglected, as the magnet flux is stationary from the rotor side.

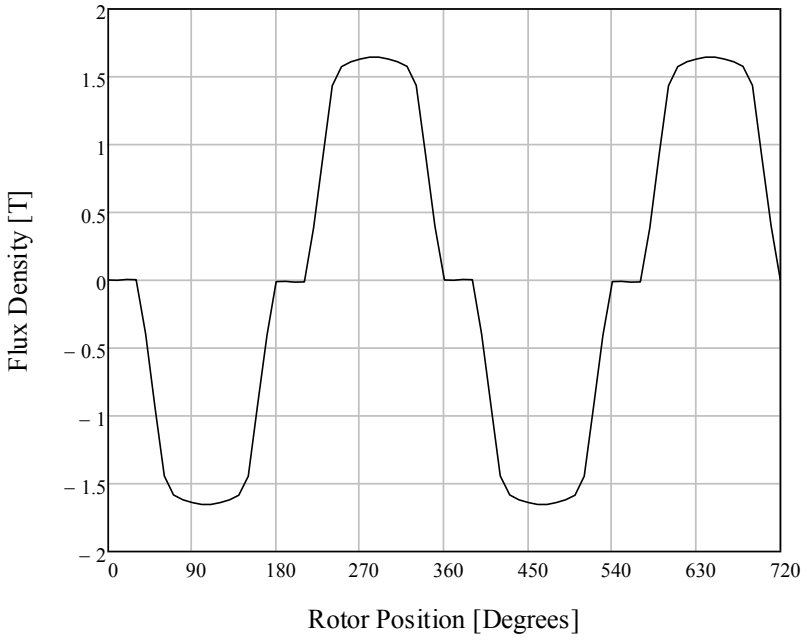

Firure 4.5: Flux density waveform in the stator tooth of the inset PM machine at no-load.

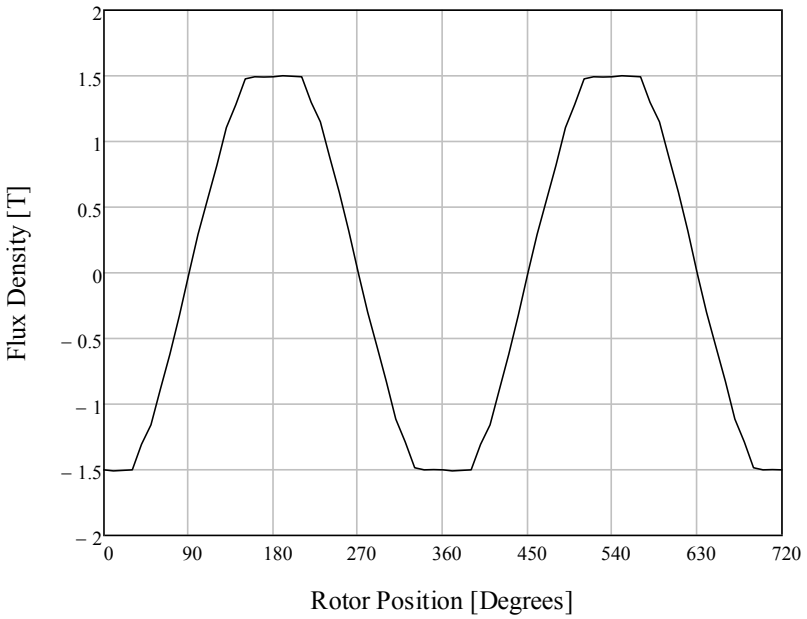

Firure 4.6: Flux density waveform in the stator yoke of the inset PM machine at no-load.

When the machine is operating under loading conditions, the flux flowing in the machine core is resultant from the reaction between the flux of the magnets, and the flux generated by the armature current. The flux generated by a certain stator current in an inset PM machine is larger than the flux generated in a surface PM machine with the same stator construction and operating with the same stator current. This is attributed to the different reluctance of the stator flux magnetic circuit. Surface PM machine has air between the magnets, while in inset PM machine this region is filled with iron, which has much larger magnetic permeability than the air. This decreases the reluctance of the stator flux magnetic path and increases the flux created by the armature winding from the same magneto motive force (mmf). The increase in the armature flux, when the machine is operating at full load, causes large deviations in the flux density waveforms in the stator laminations. However, rotor flux variation in time can still be neglected, since the

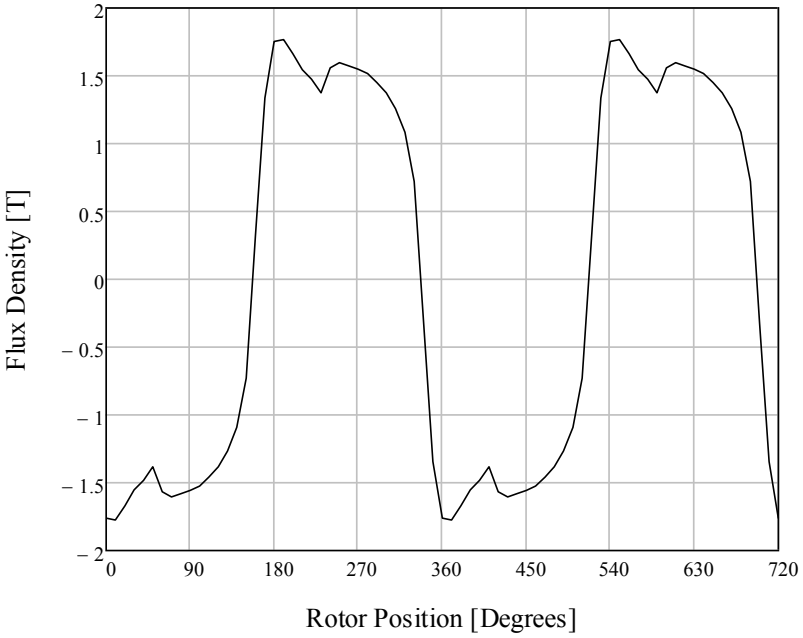

Firure 4.7: Flux density waveform in the stator tooth of the inset PM machine at full load.

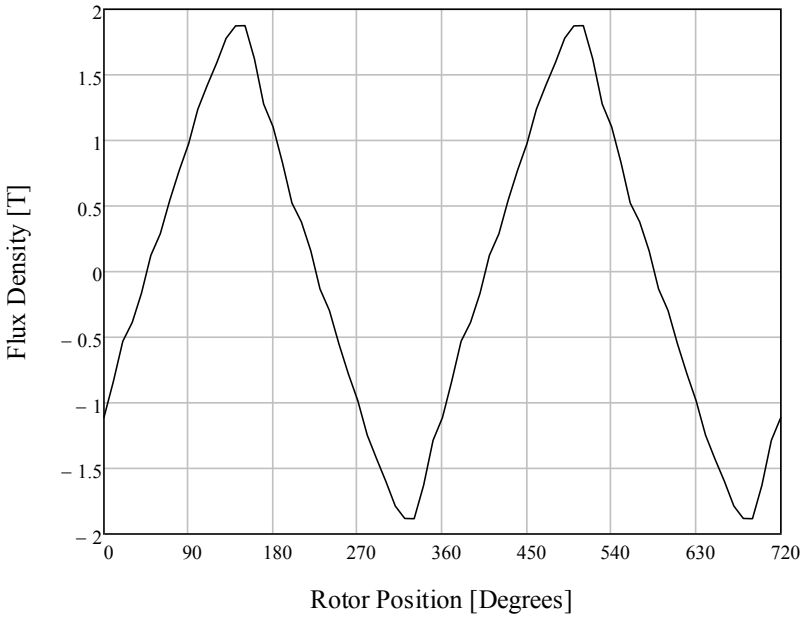

Firure 4.8: Flux density waveform in the stator yoke of the inset PM machine at full load.

stator flux is rotating at the same speed as the rotor, and therefore it can be assumed static from the rotor side. The flux density waveforms in the stator tooth and the stator yoke when the machine is operating at full load are shown in Figs. 4.7 and 4.8, respectively. It is clear that the flux density deviates in magnitude and waveform from the flux density obtained at no-load. Therefore, the simplified models for core loss modeling in PM machines which neglect the armature flux, presented in [31, 33], are not valid in the case of inset PM machines operating under loaded conditions.

4.2.2 Core Losses

The flux waveforms in the stator tooth and the stator yoke of the machine at no load and full load, displayed in Figs. 4.5-4.8, are generated in the Epstein frame laminations using the test bench. The measured core losses with these waveforms are shown in Fig. 4.9. It can be observed that the core losses measured using the PM machine flux waveforms at no-load are higher than the losses measured with sinusoidal flux at the same frequency. Also, the stator tooth flux at no-load generates higher core losses in the laminations than the stator yoke flux. From the measured losses with the flux waveforms at full load, it can be seen that there is a significant increase in the core losses measured with the stator tooth flux, which is much higher than the stator yoke losses, and the losses measured with the sinusoidal flux.

The Fourier series analysis is applied to all the flux waveforms in Figs. 4.4-4.8. The harmonic ratios of the flux waveforms are shown in Table 4.1. It can be observed that there is high harmonic content in the stator tooth flux at no-load, with the 5^{th} harmonic being 15% of the flux waveform peak. The harmonic content in the stator tooth flux

increases when the machine is operating at full load, as the 3rd and 5th harmonics are 31% and 15 % of the waveform peak, respectively.

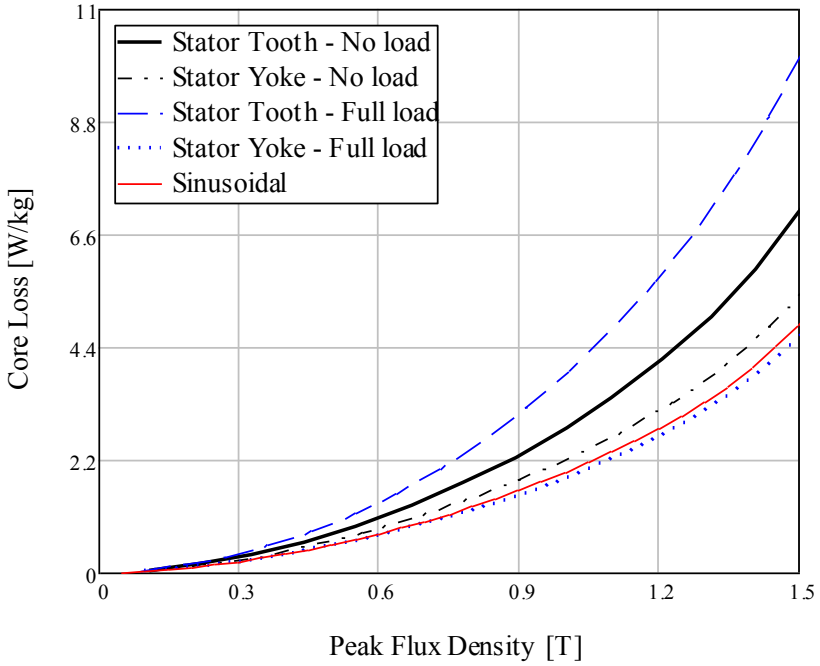

Firure 4.9: Comparison of the measured core losses with the flux waveforms in the stator tooth and the stator yoke of the inset PM machine at no-load, and full-load.

Table 4.1: Flux density harmonic ratios in the inset PM machine

Harmonic Order (h)	$\frac{B_h}{B_p}$			
	Stator Tooth No-load	Stator Yoke No-load	Stator Tooth Full-load	Stator Yoke Full-load
1	1.035	1.080	1.082	0.878
3	0.061	0.050	0.308	0.091
5	0.152	0.027	0.151	0.027
7	0.056	0.011	0.051	0.012
9	0.007	0.001	0.036	0.010
11	0.007	0.000	0.010	0.009
13	0.002	0.007	0.010	0.010

The core losses are estimated using the model presented in section 4.1. The total core loss is considered the addition of the hysteresis loss calculated by (4.5) and the eddy current loss calculated by (4.4). The first 13th harmonics are used for the eddy current loss determination. Figs. 4.10-4.13 compare the calculated core losses with the measured losses for the flux waveforms in Figs. 4.5-4.8, when the machine is running at 1912 rpm. It is clear that the calculated losses are in excellent agreement with the measured losses for the four flux waveforms. It also can be observed that the increase in the losses measured by the stator tooth flux is mainly attributed to the increase in the eddy current loss component caused by the high harmonic content in the stator tooth flux.

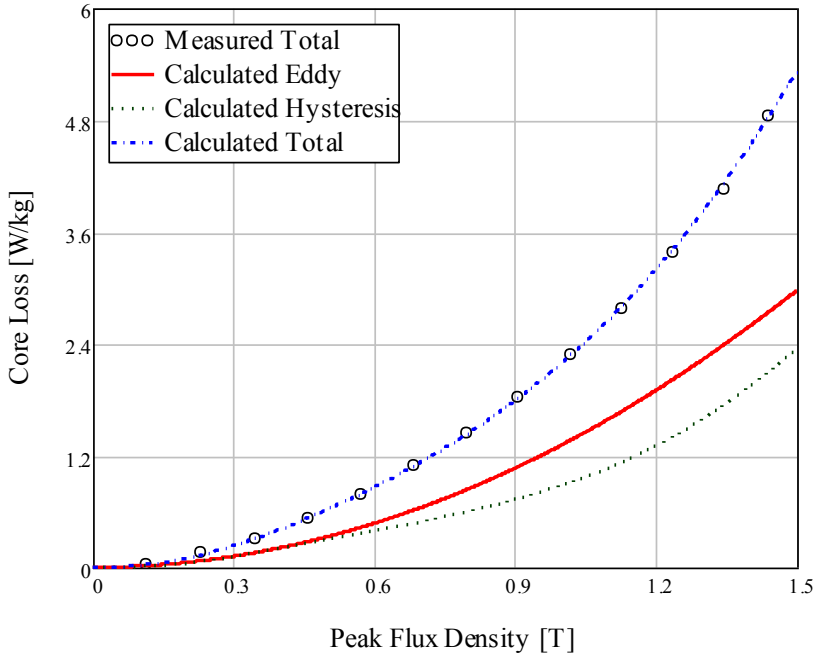

Firure 4.10: Comparison of calculated and measured core losses for the flux waveform in the stator yoke of the inset PM machine at no-load.

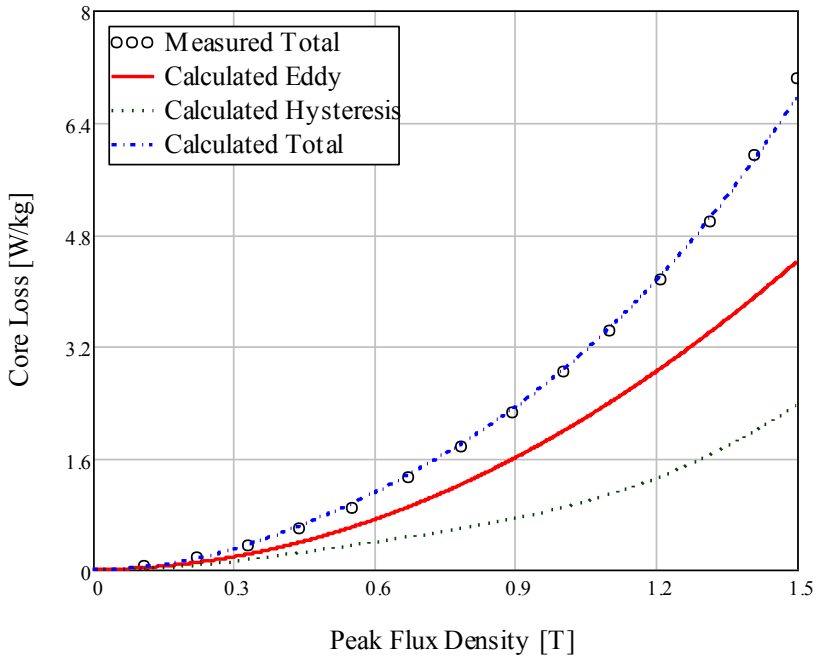

Firure 4.11: Comparison of calculated and measured core losses for the flux waveform in the stator tooth of the inset PM machine at no-load.

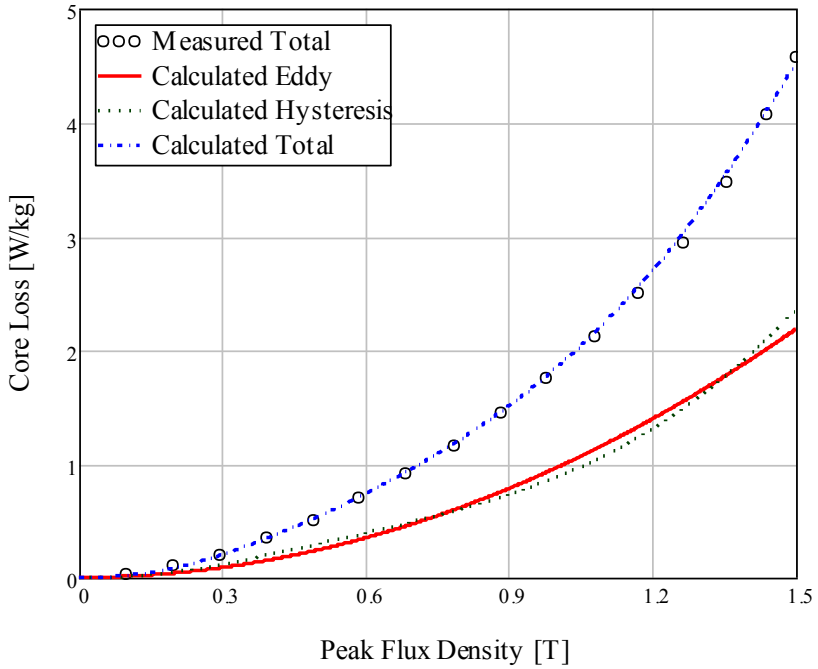

Firure 4.12: Comparison of calculated and measured core losses for the flux waveform in the stator yoke of the inset PM machine at full-load.

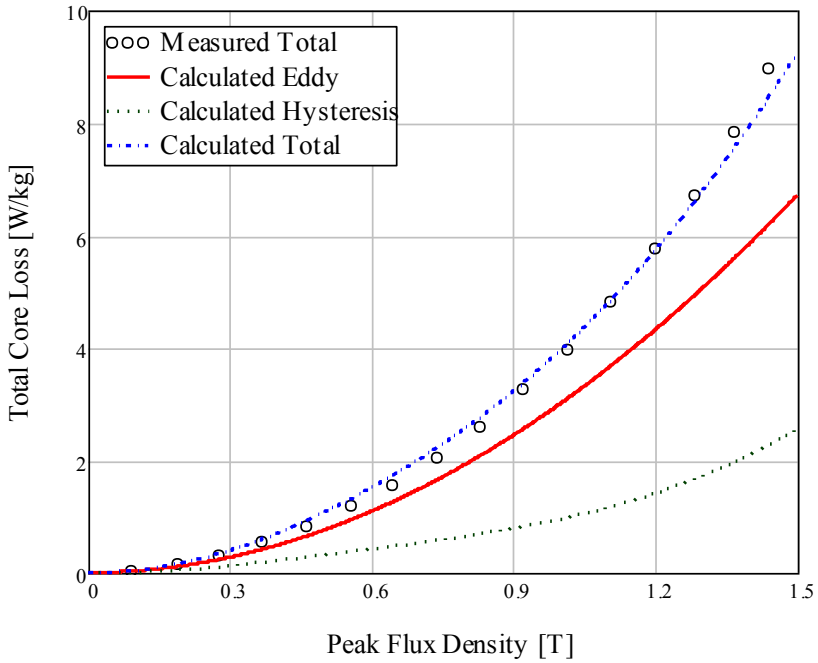

Firure 4.13: Comparison of calculated and measured core losses for the flux waveform in the stator tooth of the inset PM machine at full-load.

4.3 Core Losses in Switched Reluctance (SR) Machines

The difficulty of core loss prediction in SR machines is attributed to the nature of flux, as the flux waveforms are non-sinusoidal, and vary in different parts of the machine. The flux waveforms also change with the machine configuration, e.g., number of stator poles, rotor poles, and number of phases. In addition, the flux waveforms inside the machine are affected by the operating conditions, such as operating speed, commutation conditions, and the current waveforms [34-38].

4.3.1 Flux Waveforms

Fig. 4.14 shows the flux distribution of a 6/4 SRM when the machine is operating at 900 rpm. The flux density variation in time at a certain mesh element is obtained from the simulation results at different rotor positions. In some parts of the machine, the flux

does not only vary in magnitude, but the variation also includes the change of flux angle relative to a localized reference axis [37]. Since the test bench uses the Epstein frame for core loss measurements, it cannot be used to measure this kind of rotational core loss. The Epstein frame can only measure the core loss under alternating flux in one direction. Therefore, the flux analysis is simplified by only considering the magnitude variation of the flux density, with the flux direction defined by a reference axis that is dependent on the position of the mesh element. The flux density direction can be assumed radial in the stator pole and rotor pole, and circumferential in the stator core and rotor core [37]. Therefore, the two orthogonal flux density components B_x and B_y at a certain mesh element are resolved into radial and circumferential components depending on the position of the mesh element. The direction of the flux in the stator and rotor pole is defined by the sign of the radial flux component, and flux direction in the stator and rotor core is defined by the sign of the circumferential flux component.

Figs. 4.15-4.18 show the calculated flux density waveforms in different parts of the machine when it is running at 900 rpm. As shown in Fig. 15, the flux density waveform in the middle of the stator pole is almost unipolar, with some fluctuations in the negative direction. These fluctuations occur when the phase is turned off, and the other phases are conducting. During this period, the flux density direction is almost circumferential. It can be observed from the stator core flux waveforms, shown in Fig. 4.16, that there is also a small DC component in the stator core flux. From Figs. 17 and 18, it can be seen that the flux waveforms in the machine rotor are symmetric and do not include any DC component. Also, the rotor flux differs in magnitude and waveform from the rotor pole to the rotor core.

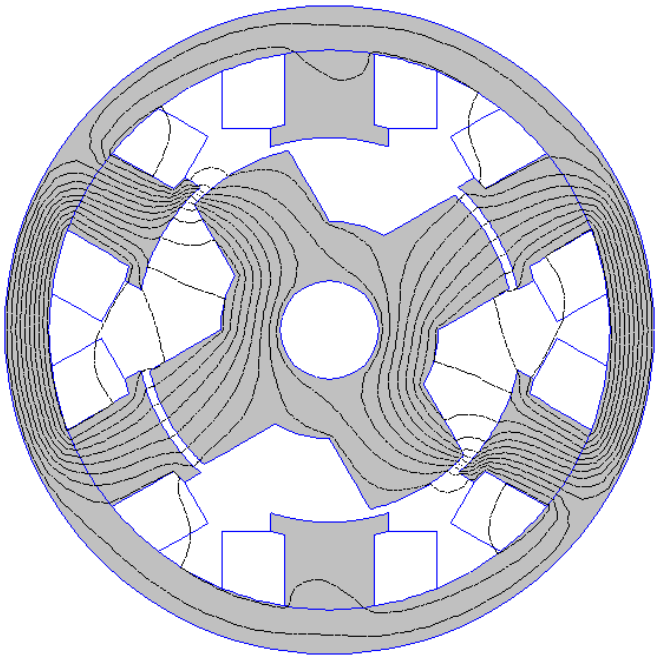

Firure 4.14: Flux distribution of a 6/4 SRM running at 900 rpm.

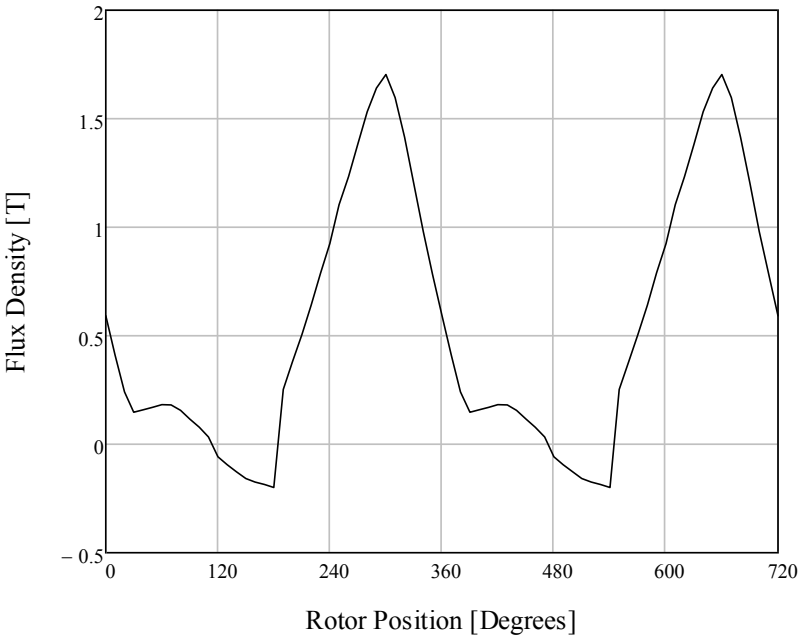

Firure 4.15: Flux density waveform in the stator pole of a 6/4 SRM.

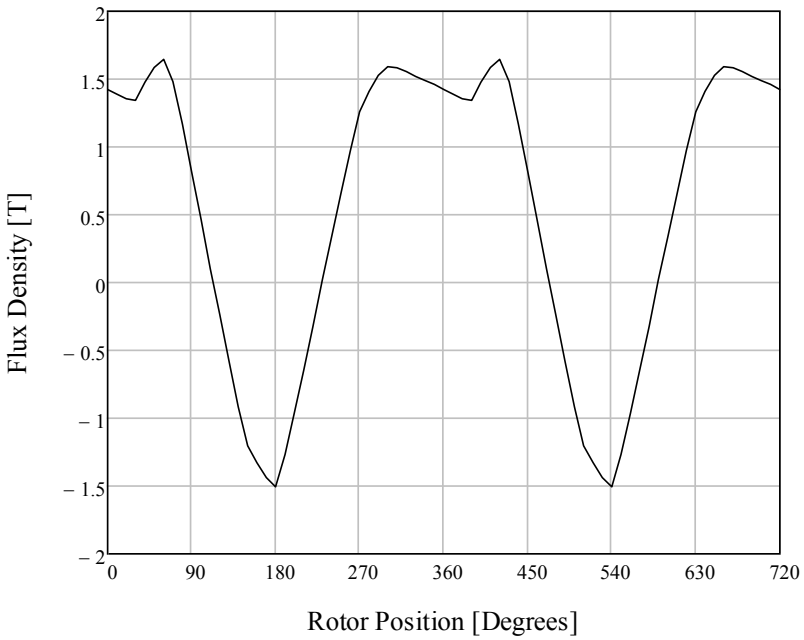

Firure 4.16: Flux density waveform in the stator core of a 6/4 SRM.

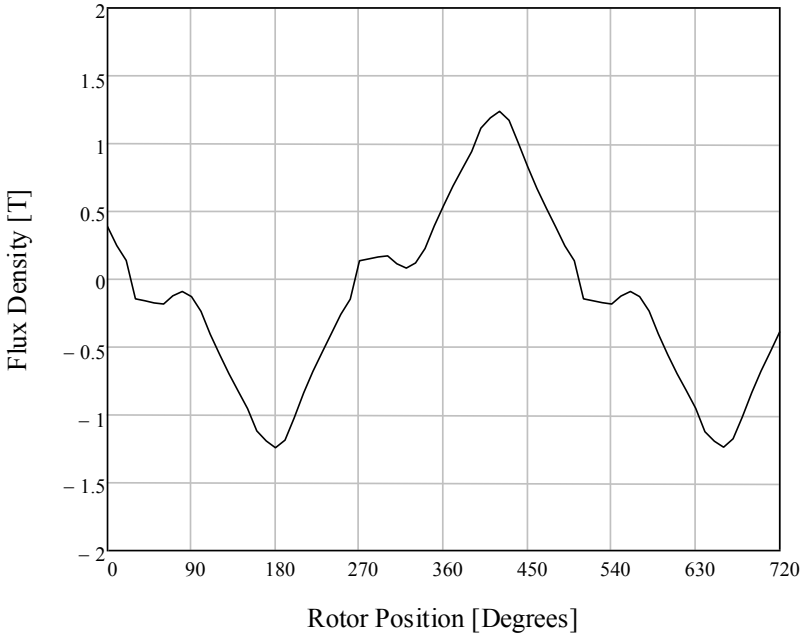

Firure 4.17: Flux density waveform in the rotor pole of a 6/4 SRM.

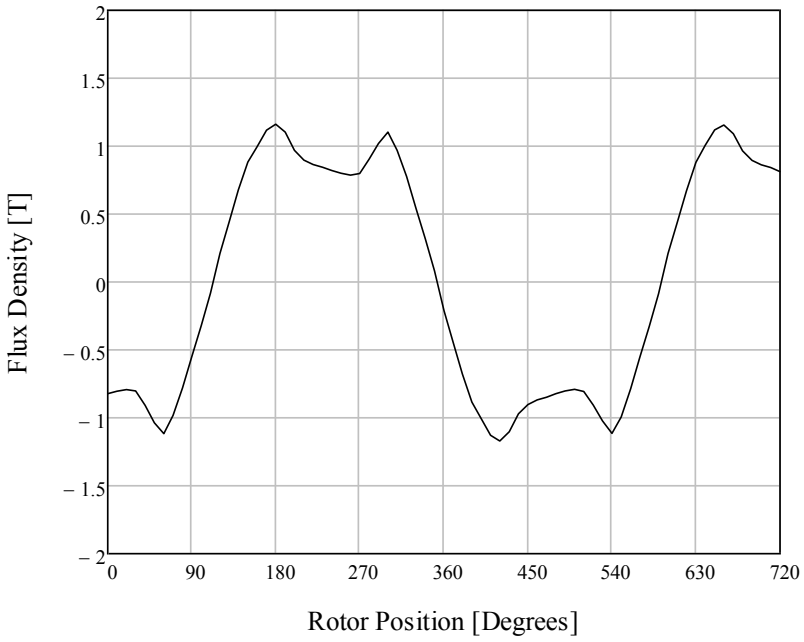

Firure 4.18: Flux density waveform in the rotor core of a 6/4 SRM.

4.3.2 Core Losses

The Fourier series analysis is applied to the SR flux waveforms, shown in Figs. 4.15-18. Table 4.2 shows the ratios of peak harmonics to the waveform peak for the flux waveforms in different parts of the machine. The stator flux has a fundamental frequency of 60Hz, while the fundamental frequency is 45Hz for the rotor flux. From table 4.2, it is observed that the 1st harmonic of the stator pole flux, is equal to 46% of the peak flux, and the 2nd harmonic is 16% of the peak flux. The 1st and 2nd harmonics are also the dominant frequencies in the stator core flux as they are 87% and 33% of the peak flux. For the rotor flux, it is observed that the 1st and 3rd harmonics are dominant. The ratios of the 1st and 3rd harmonics to the peak flux are 73% and 23% in the rotor pole, and the ratios are 98% and 30% in the rotor core flux.

Table 4.2: Flux density harmonic ratios in a 6/4 SR machine

Harmonic Order (h)	$\frac{B_h}{B_p}$			
	Stator Pole	Stator Core	Rotor Pole	Rotor Core
1	0.460	0.866	0.730	0.977
2	0.162	0.330	0.000	0.001
3	0.055	0.035	0.238	0.299
5	0.019	0.035	0.023	0.025
7	0.017	0.014	0.042	0.040
9	0.006	0.002	0.005	0.023

The DC component in the stator flux complicates the measurement of core losses, as it is impossible to measure the DC component of the flux in the Epstein frame laminations from the induced secondary voltage, which is generated by the flux rate of change. Due to the difficulties associated with core loss measurements with DC component, core loss measurements are only performed using the rotor flux waveforms. These flux waveforms are generated in the Epstein frame laminations using the test bench. Fig. 4.19 shows the measured core losses when the laminations are exposed to the flux waveforms in different parts of the rotor. It is clear that the losses measured in the laminations exposed to the flux waveforms in the SR machine rotor are higher than the losses measured with sinusoidal flux at the same frequency. Also, the rotor core flux generates higher losses in the laminations than the rotor pole flux.

The measured losses are also compared with the calculated losses by (4.4) and (4.5). Figs. 4.20 and 4.21 compare the measured and calculated losses for the rotor pole and rotor core flux, respectively. It can be seen that the calculated core losses are in good agreement with the measured losses. From Figs. 4.20 and 4.21, it is observed that the higher losses measured with the rotor core flux are mainly attributed to the higher eddy

current loss, due to the higher harmonic content in the rotor core flux. Also, the fluctuations in the rotor core flux generate minor hysteresis loops. These also increase the hysteresis losses in the rotor core.

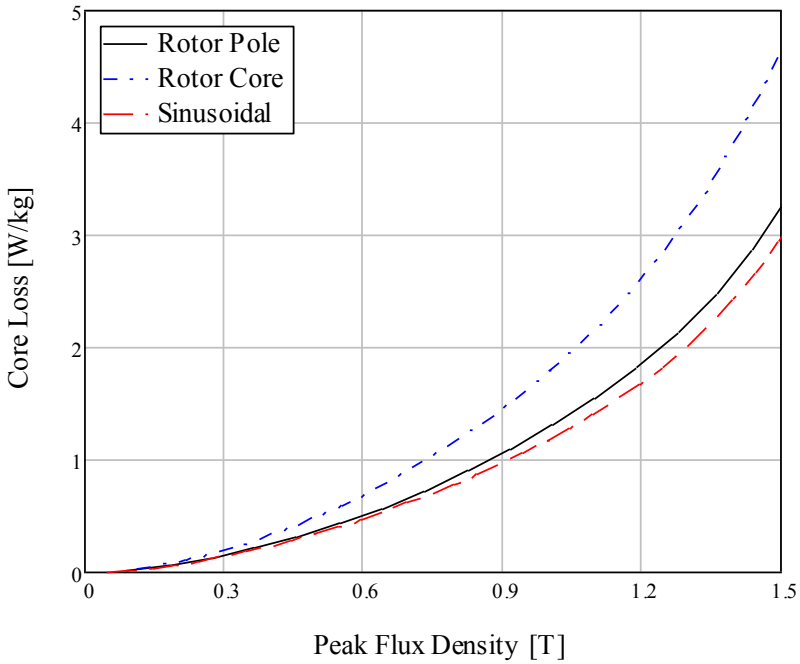

Firure 4.19: Comparison of the measured core losses with the flux waveforms in the rotor pole and rotor core of a 6/4 SR machine.

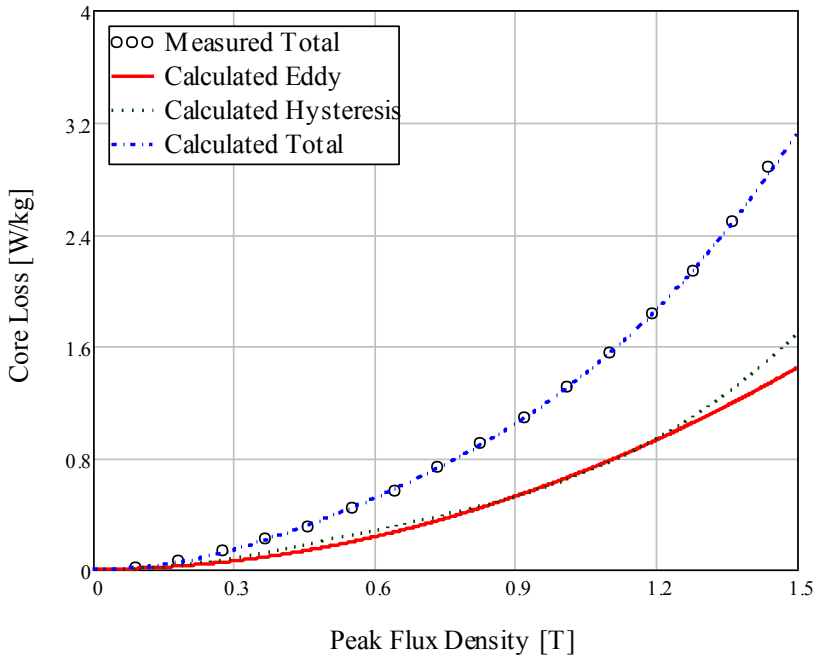

Firure 4.20: Comparison of calculated and measured core losses for the flux waveform in the rotor pole of a 6/4 SR machine.

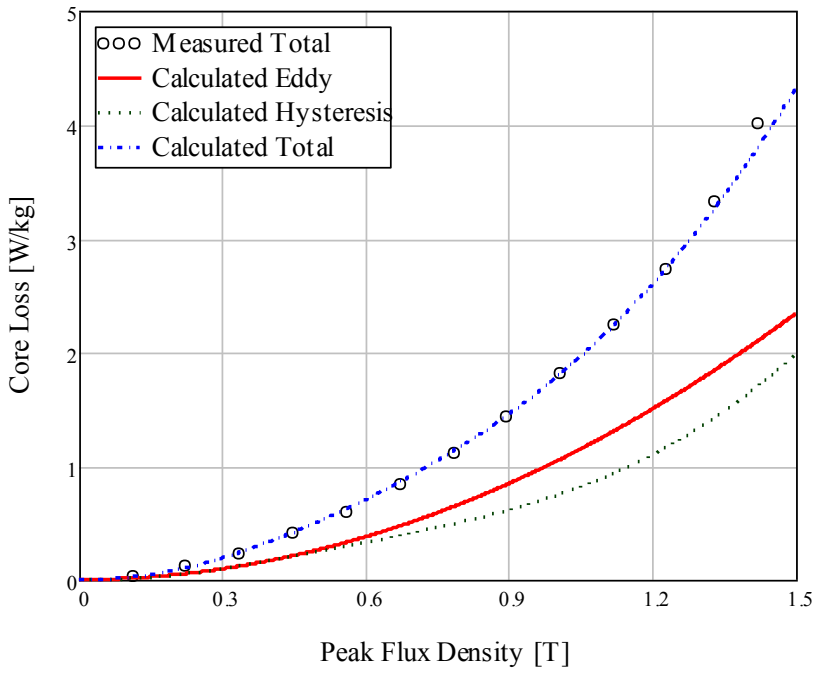

Firure 4.21: Comparison of calculated and measured core losses for the flux waveform in the rotor core of a 6/4 SR machine.

4.4 Summary

A physics based core loss model is developed to calculate the losses in machine laminations exposed to non-sinusoidal flux. The developed model takes into account the non-uniform distribution of magnetic field inside the lamination. The results are verified experimentally by measuring the core losses in laminations exposed to the flux waveforms in an inset permanent magnet (PM) machine, and a 6/4 SR machine. The flux waveforms in different sections of the machines are obtained using FE simulation. The comparison between measured and calculated core losses shows excellent agreement, confirming the validity of the model.

Chapter 5
Conclusions and Future Work

5.1 Conclusions

Core loss measurements over a wide range of frequencies are performed using the three standardized test fixtures: Epstein frame, toroid tester and single sheet tester. The discrepancies in the measured core losses and permeability amongst the three testers are shown and analyzed. The toroid tester with reduced sample size is found to produce higher losses than the Epstein frame and the single sheet tester for all the tested frequencies. Also, the measured permeability by the toroid tester is lower than the permeability measured by the other two testers. While the core losses measured by the Epstein frame and the single sheet tester are in good agreement, deviations are found in the measured magnetic permeability. These results show that the core loss measurements are strongly affected by the sample size as well as the measurement technique.

Based on the understanding of the magnetic material behavior at high frequencies, an analytical model is presented to study the influence of magnetic field distribution on the hysteresis losses in laminations exposed to high frequency excitations. The model results show that the hysteresis energy loss per cycle is dependent on skin effect, and therefore the magnetic field frequency. These results highlight that the common assumption of the hysteresis energy loss being independent of the frequency is not true when skin effect is pronounced at high frequency. The model presents a fast and efficient method of core loss separation. The developed model is then employed to separate the measured core losses in annealed and un-annealed laminations at several frequencies into the hysteresis and eddy current loss components. The annealing process is found to

reduce the hysteresis losses and improve the magnetic properties of the laminations. However, it increases the eddy current losses at high frequencies and high flux densities.

Since the flux waveforms in many electrical machines are distorted, a test bench is developed at Concordia University to carry out core loss measurements in laminations exposed to non-sinusoidal flux. The flux waveforms in different sections of an inset PM machine are obtained using FE simulation. Core loss measurements with the flux waveforms in the stator tooth and the stator yoke of the machine show a significant increase in the specific core losses in the stator tooth, especially when the machine is operating under load. Also, the flux waveforms in a 6/4 SR machine are calculated by FE simulation. Core loss measurements performed using the flux waveforms in the rotor pole and the rotor core of the machine show that the measured specific core losses in the laminations subjected to the rotor core flux are higher than the losses measured with the rotor pole flux. Also, for both the inset PM machine, and the 6/4 SR machine, large deviations are found between the core losses measured with sinusoidal flux and the core losses measured with the simulated flux waveforms in the machines. Therefore, a physics based core loss model is developed to predict the core losses in machine laminations exposed to non-sinusoidal flux. The model results for various flux waveforms in PM and SR machines are compared to the measured losses with the same flux waveforms. The calculated losses are found to be in excellent agreement with the measured losses for all the tested waveforms.

5.2 Future Work

- The finite section method, presented in Section 3.2, can be used to develop a hysteresis loss formula that accounts for the variation of the hysteresis energy loss with frequency.
- Integration of the developed core loss model, presented in Section 4.1, into FE machine design software.
- Developing a test system that can measure the flux DC component.
- Conduct further investigations on the modeling of minor hysteresis loops.
- Study the effect of punching process on the core loss in electrical machine laminations.

References

[1] P. Waide and C. U. Brunner, "Energy-Efficiency Policy Opportunities for Electric Motor-Driven Systems," *International Energy Agency*, 2011.

[2] G. A. McCo et al, "Energy-Efficient Electric Motor Selection Handbook," Revision 3, January 1993.

[3] C. P. Steinmetz, "On the law of hysteresis (originally published in 1892)," *Proc. IEEE*, vol. 72, no. 2, pp. 196-221, Feb. 1984.

[4] G. Bertotti, "General properties of power losses in soft ferromagnetic materials," *IEEE Trans. Magn.* Vol. 24, pp. 621-630, January1988.

[5] Y. Chen and P. Pillay, "An improved formula for lamination core loss calculations in machines operating with high frequency and high flu density excitation," *IEEE 37th IAS Annual Meeting*, vol. 2, pp. 759– 766, 13-18 Oct 2002.

[6] D. M. Ionel, M. Popescu, S. J. Dellinger, et al., "on the variation with flux and frequency of core loss coefficients in electrical machine," *IEEE Trans. Magn* Vol. 42, No. 3, pp. 658-666, May/June 2006.

[7] Y. Zhang, M.-C Cheng, P. Pillay, "Magnetic Characteristics and Excess Eddy Current Losses," in proc. *IEEE Industry Applications Society Annual Meeting,* 2009., pp. 1-5.

[8] I. Mayergoyz and C. Serpico, "Nonlinear diffusion of electromagnetic fields and excess eddy current losses," *J. Appl. Phys.* 85, 4910 (1999).

[9] C. Serpico, C. Visone, I. Mayergoyz et al., "Eddy current losses in ferromagnetic laminations," *J. Appl. Phys.* 87, 6923 (2000).

[10] Y. Zhang, R. Guan, P. Pillay, and M.C Cheng, "General core loss models on a magnetic lamination," in proc. *IEEE Int. Electric Machines and Drives Conf.* , 3-6 May 2009, pp. 1529 – 1534,

[11] Standard Test Method for Alternating-Current Magnetic Properties of Materials at Power Frequencies Using Wattmeter-Ammeter-Voltmeter Method and 25-cm Epstein Test Frame, ASTM Standard A343/A343M-03, 2003.

[12] Standard Test Method for Alternating-Current Magnetic Properties of Materials Using the Wattmeter-Ammeter-Voltmeter Method, 100 to 10 000 Hz and 25-cm Epstein Frame, ASTM Standard A348/A348M-00, 2000.

[13] Standard Test Method for Alternating-Current Magnetic Properties of Toroidal Core Specimens Using the Voltmeter-Ammeter-Wattmeter Method, ASTM Standard A927/A927M-99, 1999.

[14] Standard Test Methods for Alternating-Current Magnetic Properties of Materials at Power Frequencies Using Sheet-Type Test Specimens, ASTM Standard A0804/A0804M-04.

[15] P. Beckley, Electrical Steels: A Handbook for Producers and Users. Newport, U.K.: European Electrical Steels, 2000.

[16] L. T. Mthombeni, and P. Pillay, "Core Losses in Motor Laminations Exposed to High-Frequency or Nonsinusoidal Excitation*," IEEE Trans. On Ind. App.*, Vol. 40, No. 5, Sep. /Oct. 2004.

[17] A. Boglietti, P. Ferraris, M. Lazzari, and M. Pastorelli, "About the Possibility of Defining a Standard Method for Iron Loss Measurements in Soft Magnetic

Materials with Inverter Supply," *IEEE Trans. Magn.*, vol. 33, pp. 1283–1288, Sept.–Oct. 1997.

[18] T. L. Mthombeni, P. Pillay, R. M. W. Strnat, "New Epstein Frame for Lamination Core Loss Measurements Under High Frequencies and High Flux Densities," *IEEE Transactions on Energy Conversion*, Vol. 22, Issue 3, Sept. 2007, pp. 614 – 620.

[19] M. Manyage, P. Pillay, "New Epstein Frame for Core Loss Measurements at High Frequencies and High Flux Densities," in proc. IEEE Int. *Industry Applications Society Annual Meeting*, 2008, pp. 1 – 6.

[20] A. Boglietti, A. Cavagnino, M. Lazzari, and M. Pastorelli, "The Annealing Influence onto Magnetic and Energetic Properties in Soft Magnetic Material after Punching Process," in Proc. *IEEE Int. Electric Machines and Drives Conf.,* vol. 1, June 1–4, 2003, pp. 503–508.

[21] A. Boglietti, A. Cavagnino, "Iron Loss Prediction with PWM Supply: An Overview of Proposed Methods from an Engineering Application Point of View," in proc. *IEEE Int*. *Industry Applications Society Annual Meeting*, 2007, pp. 81 – 88.

[22] B. D. Cullity and C. D. Graham, "Introduction To Magnetic Materials," 2nd ed. John Wiley & Sons, 2009.

[23] Y. Zhang, M-C. Cheng, P. Pillay and B. Helenbrook, " High order finite element model for core loss assessment in a hysteresis magnetic lamination," *J. Appl. Phys.* 106, 43911 (2009).

[24] Y. Zhang, "Experimental, Theoretical and Numerical Investigations of Core Losses in Laminated Magnetic Materials," PhD Thesis, Clarkson University, Nov., 2008.

[25] H. Hauser, “Energetic model of ferromagnetic hysteresis: Isotropic magnetization,” *J. Appl. Phys.* 96, 2753 (2004).

[26] T.L.Mthombeni and P.Pillay, "Physical Basis for the Variation of Lamination Core Loss Coefficients as a Function of Frequency and Flux Density,” *IECON,* France, 2006.

[27] R. H. Pry and C. P. Bean, “Calculation of the energy loss in magnetic sheet materials using a domain model,” *J. Appl. Phys.*, vol. 29, pp. 532–533, Mar. 1958.

[28] P. Beckley, Electrical Steels for Rotating Machines: IET Power and Energy Series, 37, 2002.

[29] A. Boglietti, A. Cavagnino, M. Lazzari, and M. Pstorelli, “Predicting iron losses in soft magnetic materials with arbitrary voltage supply: an engineering approach,” *IEEE Trans. Magn.,* vol. 39, no. 2, pp. 981 - 989, Mar. 2003.

[30] J. D. Lavers, P. P. Biringer, and H. Hollitscher, “A simple method of estimating the minor loop hysteresis loss in thin laminations,” *IEEE Trans. Magn.*, vol. MAG-14, no. 5, pp. 386–388, Sep. 1978.

[31] G. R. Slemon and X. Liu, “Core losses in permanent magnet motors,” *IEEE Trans. Magn.*, vol. 26, pp. 1653 – 1655, September 1990.

[32] M. Manyage, "Traction Motor Design,” PhD Thesis, University of Cape Town, June, 2008.

[33] M. Chunting, G.R. Slemon, R. Bonert, “Modeling of iron losses of permanent-magnet synchronous motors,” *IEEE Transactions on Industry Applications*, vol. 39, pp. 734 – 742, May-June 2003.

[34] P. Materu and R. Krishnan, “Estimation of switched reluctance motor losses,” in proc. *IEEE Ind. Appl. Soc. Annu. Meeting*, vol. 1, Oct. 2–7, 1988, pp. 79–90.

[35] J. Faiz and M. B. B. Sharafin, “Core losses estimation in a multiple teeth per stator pole switched reluctance motor,” *IEEE Trans. Magn.*, vol. 30, no. 2, pp. 189–195, Mar. 1994.

[36] Y. Hayashi and T. J. E. Miller, “A new approach to calculating core losses in the SRM,” *IEEE Trans on. Ind. Appl*., vol. 31, no. 5, pp. 1039–1046, Sep./Oct. 1995.

[37] S.D. Calverley, G.W. Jewell, R.J. Saunders, “Prediction and Measurement of Core Losses in a High-Speed Switched-Reluctance Machine,” *IEEE Trans. Magn*., Vol. 41 , pp. 4288 – 4298, Nov. 2005.

[38] T. L. Mthombeni and P. Pillay, “Lamination Core Losses in Motors with Nonsinusoidal Excitation with Particular Reference to PWM and SRM excitation waveforms,” *IEEE Transactions on Energy Conversion*, vol. 20, pp. 836 – 843, December 2005.